Journal of Geochemical Exploration 158 (2015) 55–73

Contents lists available at ScienceDirect

Journal of Geochemical Exploration

journal homepage: www.elsevier.com/locate/jgeoexp

Discovery of Au–Ag mineralization by stream sediment and soil geochemical exploration in metamorphic terrain in western Turkey

Huseyin Yilmaz [a,*], Fatma Nuran Sonmez [a], Emmanuel John M. Carranza [b]

[a] Department of Geological Engineering, Faculty of Engineering, Dokuz Eylul University, Tinaztepe, Buca 35160, Izmir, Turkey
[b] Department of Earth and Oceans, College of Science, Technology and Engineering, James Cook University, Townsville 4811, Queensland, Australia

ARTICLE INFO

Article history:
Received 6 December 2014
Revised 18 June 2015
Accepted 5 July 2015
Available online 14 July 2015

Keywords:
Fractal analysis
BLEG
−80 mesh stream sediment
MMI
Gold discovery
Cemalcavus

ABSTRACT

Exploration based on BLEG (bulk leach extractable gold) and −80 mesh stream sediment, and soil geochemical sampling over the Usak-Esme region in western Turkey resulted in the discovery of Cemalcavus Au–Ag–As mineralization. This schistosity-controlled mineralization occurs within sericitized–chloritized almandine–amphibolite facies metamorphic rocks. No mineralization has been reported previously in the area. The concentration–area (C–A) fractal model was applied to the raw data to set threshold values defining background and anomalous classes of uni-element concentrations in BLEG and −80 mesh stream sediment samples as well as soil samples analyzed by conventional and MMI (mobile metal ion) extraction techniques. The conventional soil geochemical data failed to yield anomalies linked to gold mineralization at or close to the surface whereas the MMI soil geochemical data yielded genuine anomalies that were not only reproducible but were associated with subsurface mineralization. Thus, the MMI technique has maximized drilling efficiency at Cemalcavus Prospect by providing precise anomalies closely related to subsurface sources. As a whole, BLEG and −80 mesh stream sediment anomalies in combination with MMI soil anomalies followed-up by core drilling led to the recognition of the Cemalcavus Au–Ag prospect although an economically viable mineralization is yet to be discovered.

1. Introduction

Regional geochemical exploration based on stream sediment data is a time and cost efficient method for identifying anomalous areas especially in the initial stages of prospecting for undiscovered outcropping or concealed mineralizations (El-Makky and Sediek, 2012; Lusty et al., 2012; Yilmaz, 2003, 2007; Yousefi et al., 2013). Stream sediments remain as the predominant sampling media in regional green-field geochemical exploration of areas where topography has developed distinct drainage systems (Fletcher, 1997; Hale and Plant, 1994).

Optimizing geochemical survey design requires a balance between maximizing the length and continuity of detectable dispersion trains and minimizing cost and time requirements, a major component of which may be related to field sample collection. In the case of Au exploration, stream sediment geochemical survey can prove difficult due to the complex array of factors that control the distribution and form of Au in stream sediments, including hydraulic and chemical processes as well as the nature of the source (Cohen et al., 2004). Small-scale deviation in stream hydraulics accompanied by grain scarcity effects on sample representativity as well as sampling errors may lead to non-systematic distance versus concentration relationships and marked deviations from the idealized anomaly decay and mass balance assumptions in relatively small catchments. The mentioned factors complicate the choice of sampling media, analytical methods and setting of threshold values to separate background and anomaly (Cohen et al., 2004). With regard to improving sample representativity and reduction of detection limits, the bulk leach extractable Au (BLEG) method has been demonstrated in many previous works (e.g., Carlile et al., 1998; Leduc and Itard, 2003; Radford, 1996).

Conventional exploration geochemistry has traditionally focused on various types of secondary elemental dispersion halos at the land surface. This has been successful in discovering mineral deposits beneath relatively thin residual overburden. However, it is inefficient in finding mineral deposits hidden deeply beneath various kinds of overburden. For this reason, much attention has been directed in the last three decades or so toward development of deep-penetrating exploration geochemistry for discovery of buried mineral deposits. Several published case studies disclosed geochemical anomalies in transported overburden sitting above buried mineral deposits in different environments (e.g., Cameron et al., 2004; Cohen et al., 2010; Nyade et al., 2011). In particular, a series of approaches to extract mobile constituents from soil by selective leaching has been made (e.g., Bajc, 1997; Gray et al., 1999; Kelley et al., 2003; Mann et al., 1998, 2005).

Bajc (1997) noted that MMI (mobile metal ion) digestion was highly welcomed by the exploration community because of its successful track record in non-glaciated, arid and tropical climatic regions. Bajc (1997) clearly demonstrated that MMI and enzyme leach selective digests provided exploration geochemists with valuable geological information for

* Corresponding author.

http://dx.doi.org/10.1016/j.gexplo.2015.07.003
0375-6742/

the identification of potential exploration targets when used in conjunction with other exploration data. It was also emphasized that the MMI technique does not work well as a stand-alone method, although the Golden Web gold deposit, Coolgardie, Western Australia was discovered mainly by application of the MMI technique (Mann et al., 1998). Subsequent mining established a high correlation between the times 20 MMI Au response ratio (RR) contour and the economic mineralized envelope, located some 17–50 m beneath. Moreover, Gray et al. (1999) carried out sampling in seven different sites on the Yilgarn Craton to test the usefulness of various selective and partial extractions for Au exploration, particularly in areas covered by extensive transported overburden. They used MMI analysis consisting of two separate techniques: (i) an acid extraction for Cd, Cu, Pb and Zn, giving results that are similar to HCl and the selective extraction reagents; and (ii) MMI method using an alkaline extraction for Ag, Au, Co, Ni and Pd, which appeared to be optimized for Au and Ag; 70–80% of the total Au was dissolved in soils containing significant carbonate. Kelley et al. (2003) concluded that partial extraction geochemistry is an effective tool for detecting secondary dispersion processes. Strong evidence existed in northern Chile for the vertical migration of anomalous pathfinder elements through transported overburden. They suggested that selection of the most appropriate method should be based on the deposit type being sought, the nature of the overburden, and the stability of the leach method for this overburden. It was also emphasized that mechanical dispersion strongly influenced the results of partial extraction methods and therefore, a strong extraction method should always be used in conjunction with a partial extraction method to characterize the mechanical component in the sample. Furthermore, many elements yield significant concentrations of 'mobile

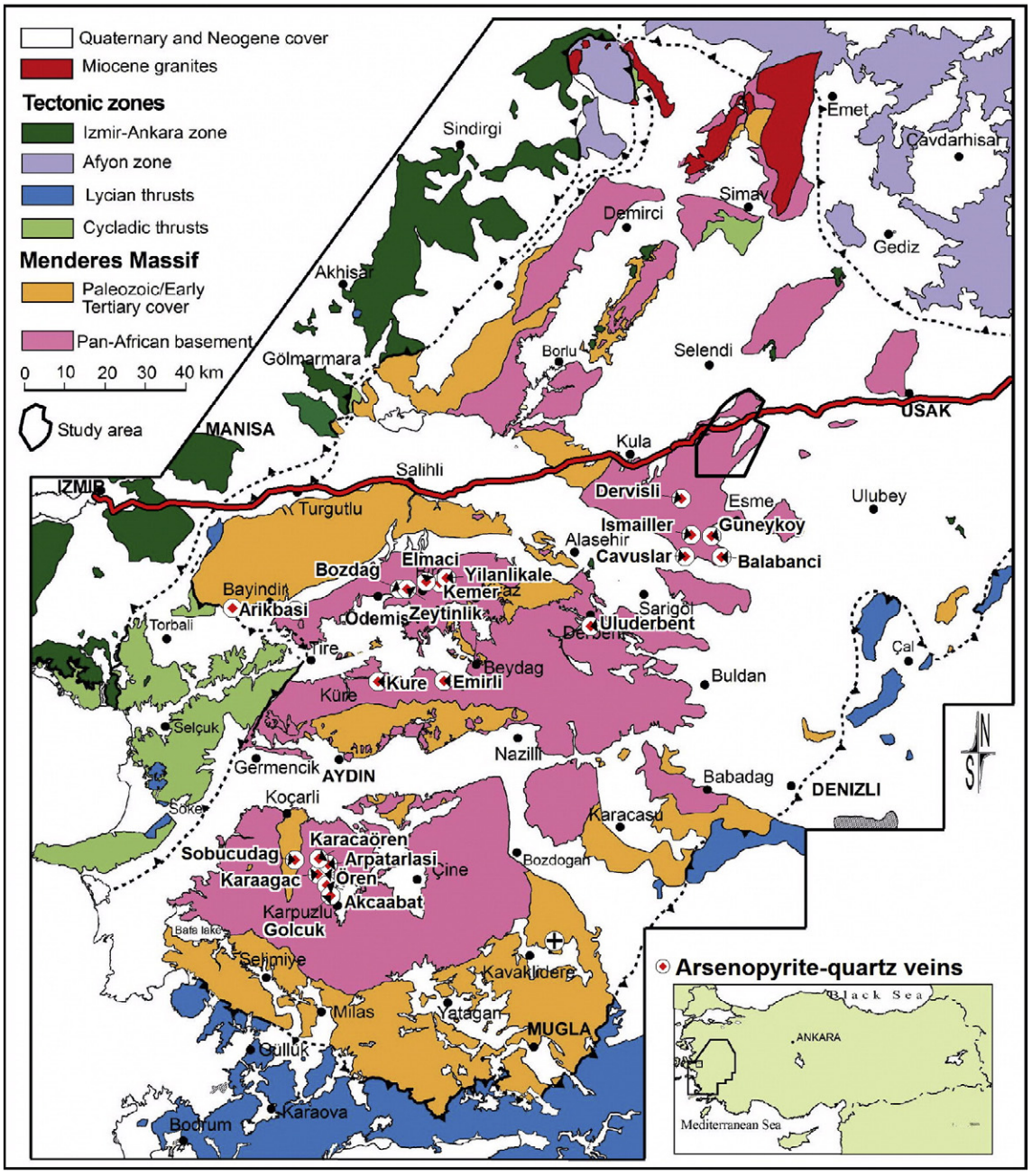

Fig 1. .Geology and mineralization map of the Menderes Massif, Turkey.
Metamorphic fields are modified from Candan et al. (2011).

ions' in the top 30 cm of the soil profile over the Nepean nickel mine in a semi-arid part of Western Australia (Mann et al., 2005).

Numerous mechanisms causing upward element migration through overburden above mineral deposits have been proposed (e.g., Cameron et al., 2002, 2004; Goldberg, 1998; Mann et al., 2005; Reith and Mcphail, 2007; Rose et al., 1979; Smee, 1983). One of these mechanisms involving mass transport by water in solution or suspension may account for the greater number of element transport in the subsurface environment (Rose et al., 1979). Other mechanisms involving the processes being active in the water-saturated zone are heat- or density-driven convection, gas bubble transport (Putikov and Wen, 2000), seismic pumping (Cameron et al., 2002; Kelley et al., 2003), electrochemical distribution (Govett, 1976; Smee, 1983), and diffusion along chemical slope. Mechanisms involving processes being active in unsaturated zones include capillary fluid migration (Mann et al., 2005), gas phase transport (Klusman, 2009), barometric pumping (Cameron et al., 2002).

In western Turkey, which is underlain mainly by blocks of crystalline metamorphic complexes, ophiolitites and volcano-plutonic rocks, exploration for gold-silver has been reported since 1988. However, although several companies have carried out intense geochemical exploration, little information on geochemical dispersion of gold-silver and other associated elements from deposits and prospects is revealed from this region (Yilmaz, 2003, 2007). As example, no significant green-field geochemical exploration activities have been reported on the northeast corner of the Menderes Metamorphic Massif, which is cut by minor sub-aerial basaltic volcanic rocks (Fig. 1).

The study area in the northeastern part of the Menderes Metamorphic Massif was selected for scrutinizing dispersion characteristics of various elements with emphasis on Au, Ag and As. The area, located west of Usak, is accessible via Izmir-Ankara highway (Fig. 1). This part of the medium- to high-grade metamorphic terrain located between Esme and Selendi was selected to conduct the first applications of exploration geochemistry including BLEG (1.2 mm), −80 mesh stream sediment, −80 mesh conventional and MMI soil geochemical sampling for discovering precious metal occurrences in western Turkey. This area in the Demirci–Gordes Submassif has no record of Au–Ag mineralization or anomalies (Fig. 1), except for the Eldorado Gold-owned, world-class Kisladag intrusive-hosted porphyry Au deposit located 10 km SE of the study area and the several Au-bearing arsenopyrite mineralizations reported by MTA (Mineral Research and Exploration Institute of Turkey) southwest of Esme–Kula (Fig. 2). The mineralization consists predominantly of Au and Ag with associated As and variable (or minor) amounts of Sb and Pb in a narrow zone of outcropping quartz-rich breccia/stockwork (0.5 km^2) within the metamorphic schists near to Cemalcavus village. However, schistosity-controlled, low-grade gold–silver mineral occurrences have been discovered in the study area by regional stream sediment survey, followed-up by detailed soil and rock chip surveys.

The work presented in this paper examines the capability of BLEG (bulk cyanide leach extractable gold of −16 mesh and −80 mesh fractions) and four-acid digested metal contents of the −80 mesh fraction of stream sediment samples. These two sampling methods as well as conventional soil sampling led to the discovery of several low- and high-grade mineralizations in western Turkey, a few of which were presented by Yilmaz (2003, 2007) and Yilmaz et al. (2013). Conventional and MMI (mobile metal ion) soil techniques, with the latter being first implemented in the study area than elsewhere in Turkey, were applied to follow-up BLEG and −80 mesh stream sediment anomalies clustered strongly over the area stretching from Gokbel to Alabasli.

2. The study area

2.1. Regional geology and mineralization

Western Turkey consists of three major tectono-lithologic slices (Fig. 1): (i) the Mesozoic Lycian nappes and the Early Bornova flysch

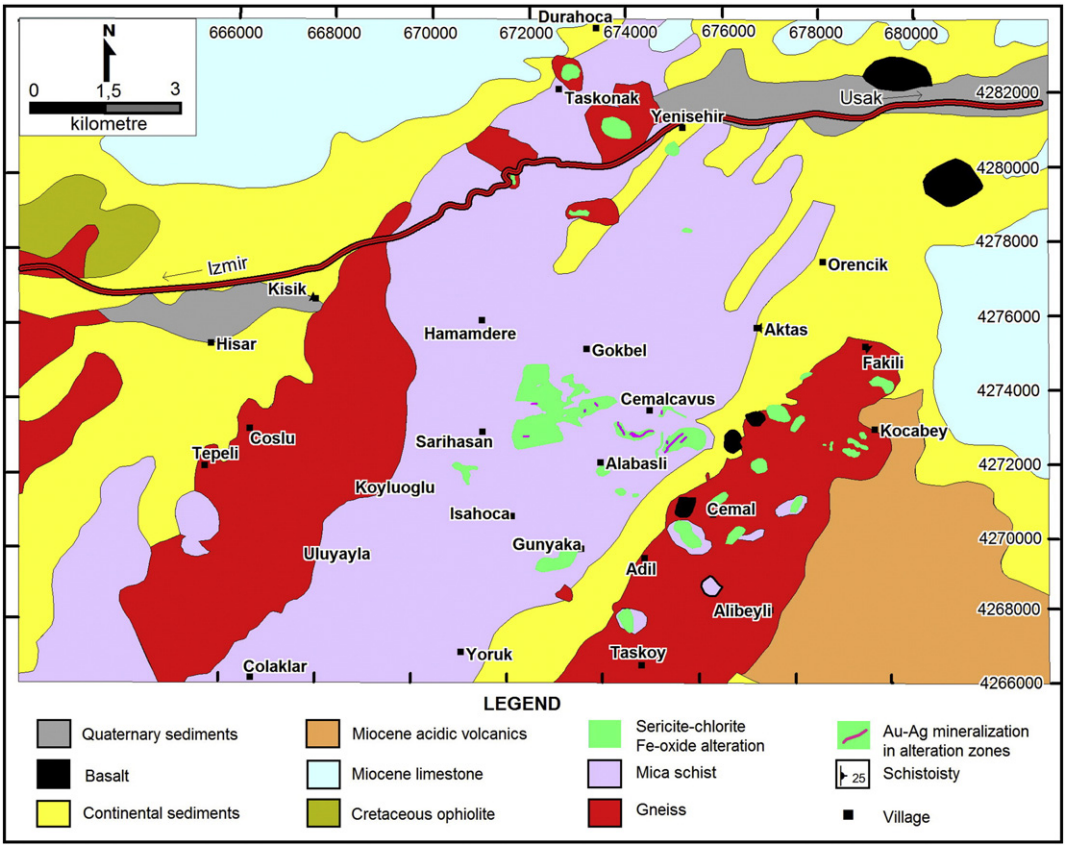

Fig. 2. Simplified bedrock geology, mineralization and alteration map of the Cemalcavus area and its surroundings.

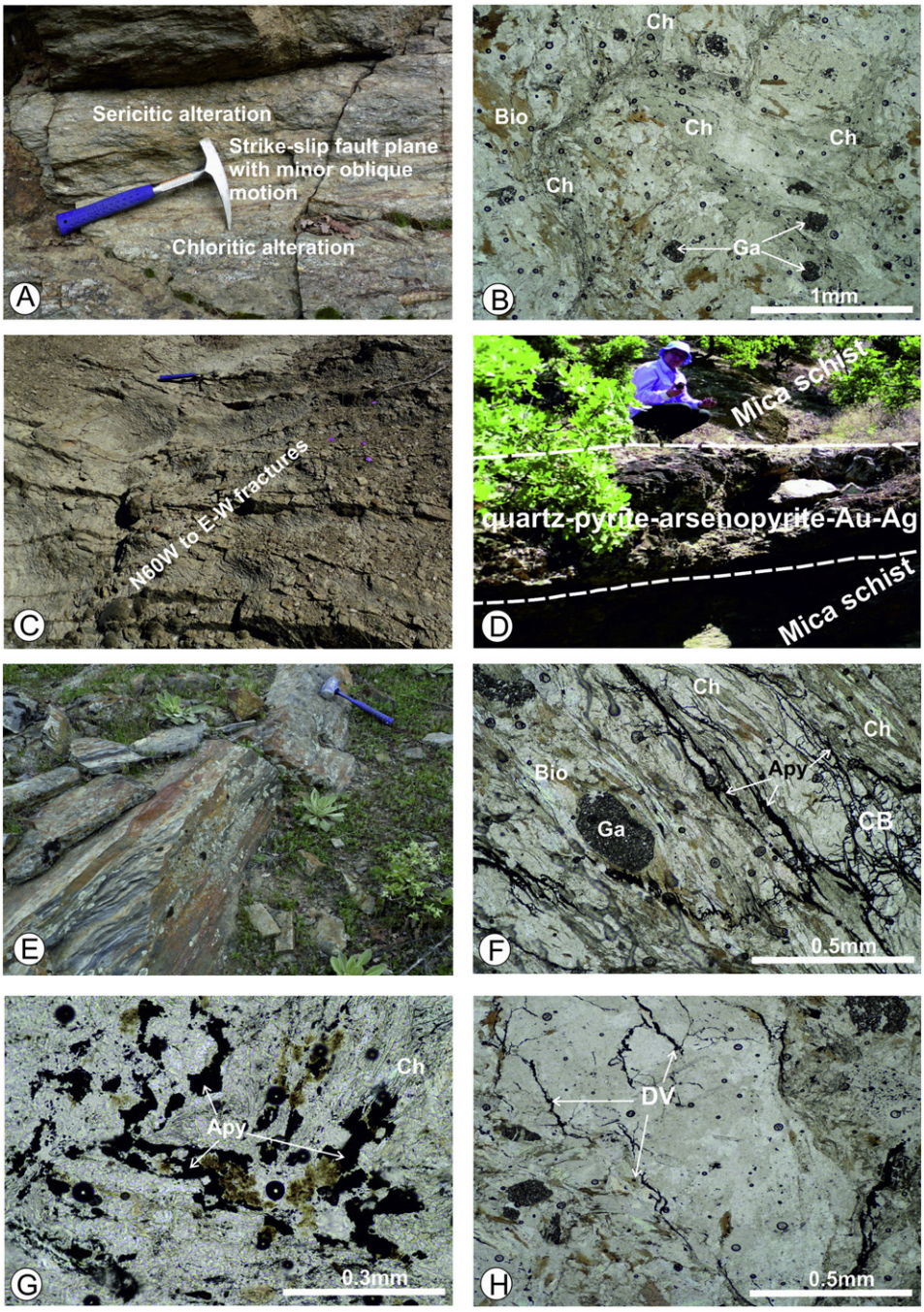

Fig. 3. Field photographs (A, C) and photomicrographs (under parallel Nichols: B, D, E, F) of alteration and mineralization: A) Sericitic and chloritic alteration on a fault surface, B) Fracture-controlled chloritic (Ch) alteration; Ga: garnet, C) N60°W and E–W trending intense fracturing, D) Dark-gray, 1.5 m thick schistosity-controlled pyrite–arsenopyrite-rich quartz-vein breccia outcrop containing 0.5 ppm Au, 21 ppm Ag and 0.5% As, E) Silicified, dark gray mica schist with schistosity-controlled Au–Ag–As–Sb mineralization containing 0.6 ppm Au, 24 ppm Ag, 2300 ppm As and 3250 ppm Sb, F) Fracture filling or crackle breccias (CB) impregnated by arsenopyrite with associated Au–Ag mineralization in chloritized matrix, G) Disseminated arsenopyrite in heavily chloritized matrix and H) Dendritic arsenopyrite (Apy) veinlets.

zone deposited during opening of the northern branch of the Neo-Tethys Ocean (Regnier et al., 2007); (ii) the Cycladic blueschist unit with Mesozoic platform carbonates and metaolistostromes; and (iii) the Menderes massif, which underlies the first two slices (Collins and Robertson, 2003; Rimmele et al., 2003, 2005).

The Menderes massif is situated between the Izmir-Ankara Mélange, a Neo-Tethyan suture zone of Cretaceous–Paleocene age, and the Permian–Eocene Lycian nappe complex that roots in this suture zone (Sengor et al., 1984; Hetzel et al., 1995, 1998; Fig. 1). It is divided by E–W-oriented Late Miocene–Pliocene graben systems into three submassifs (Candan et al., 2001; Koralay et al., 2001), namely (from north to south) the Demirci–Gordes, Odemis–Kiraz and Cine submassifs (Fig. 1). Despite its complex tectonic structure, the Menderes Massif can be divided into two main rock associations: (i) Pan-African basement rocks comprising partly migmatized Late Proterozoic clastic metasediments (Koralay et al., 2001) and (ii) core and cover rock series, the oldest of the core series are ~550 Ma granites in the southern and central submassif (Hetzel et al., 1998). These two main rock associations were intruded by leucocratic orthogneisses of Triassic age (Fig. 1) in the eastern part of the core of the Menderes Massif (Koralay et al., 2001). A three-stage

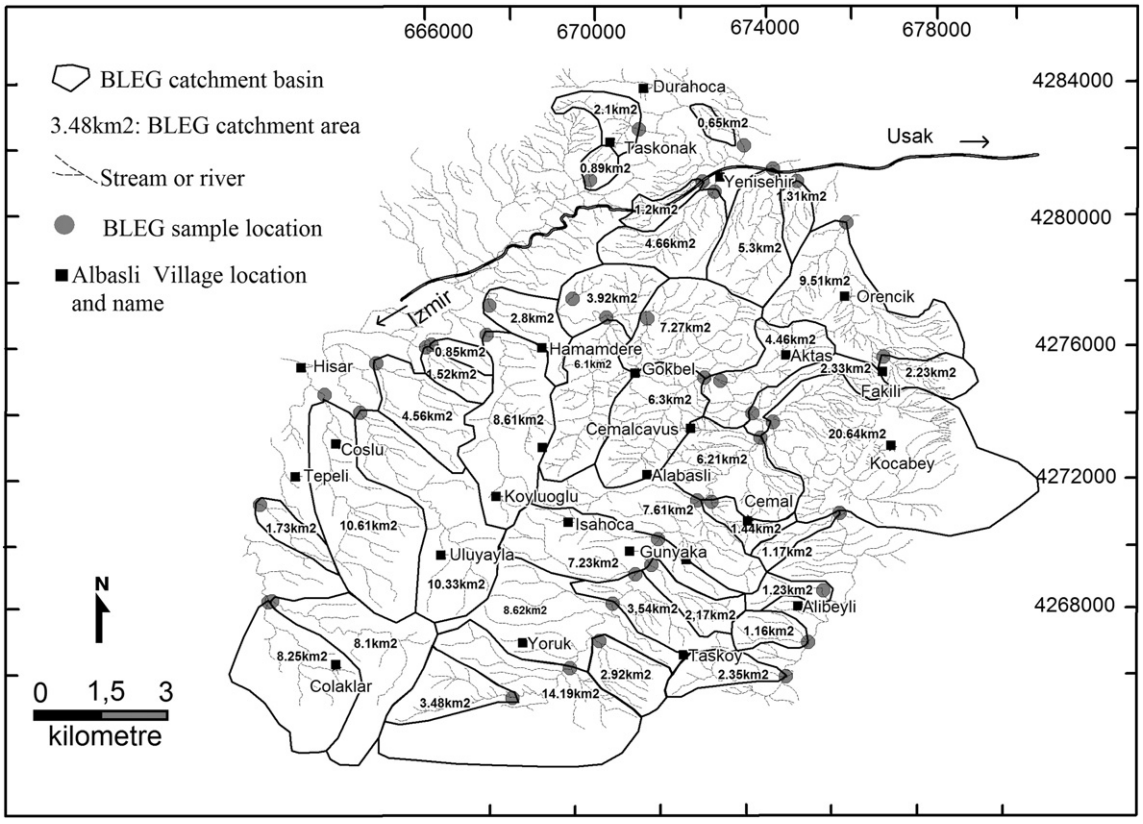

Fig. 4. Detailed BLEG stream sediment sample survey and size of drainage catchment basins from Cemalcavus area.

tectono-metamorphic model has been proposed for the evolution of the Menderes Massif, and details of this model can be found in Rimmele et al. (2003).

Within the Menderes Massif but outside the study area, several possible orogenic gold deposits have been reported (e.g., Cağatay and Eyyüboğlu, 1979; MTA, 1970, 1979; Eurogold Company (1992); Akiska et al., 2008; Sonmez, 2013). Yigit (2009) suggested that at least two different events influenced the genesis of these deposits but he emphasized the genesis of these deposit is not yet constrained by any research. Minor post-mineralization intermediate argillic alteration (10–50 m × 600 m) located 2 km NW of Albasli was located in the study area and, therefore, was not expected to cause re-distribution of the metamorphic-hosted Au and Ag.

2.2. Local geology and mineralization

The study area of ~250 km^2 (Fig. 2) is comprised mainly of Neo-Proterozoic metamorphic crystalline rocks (orthogneiss, augengneiss and gneiss-micaschist intercalations), which are tectonically overlain by Cretaceous ophiolites, which are in turn unconformably overlain by Miocene acidic volcaniclastic rocks, continental sediments, Pliocene basalt flow and breccia, and Quaternary fluvial

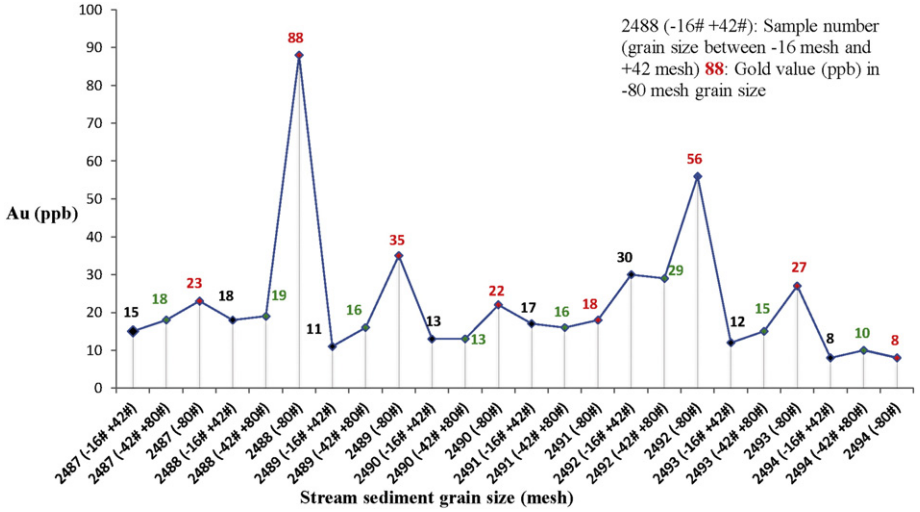

Fig. 5. Concentration versus particle size plots for the Cemalcavus area for Au.

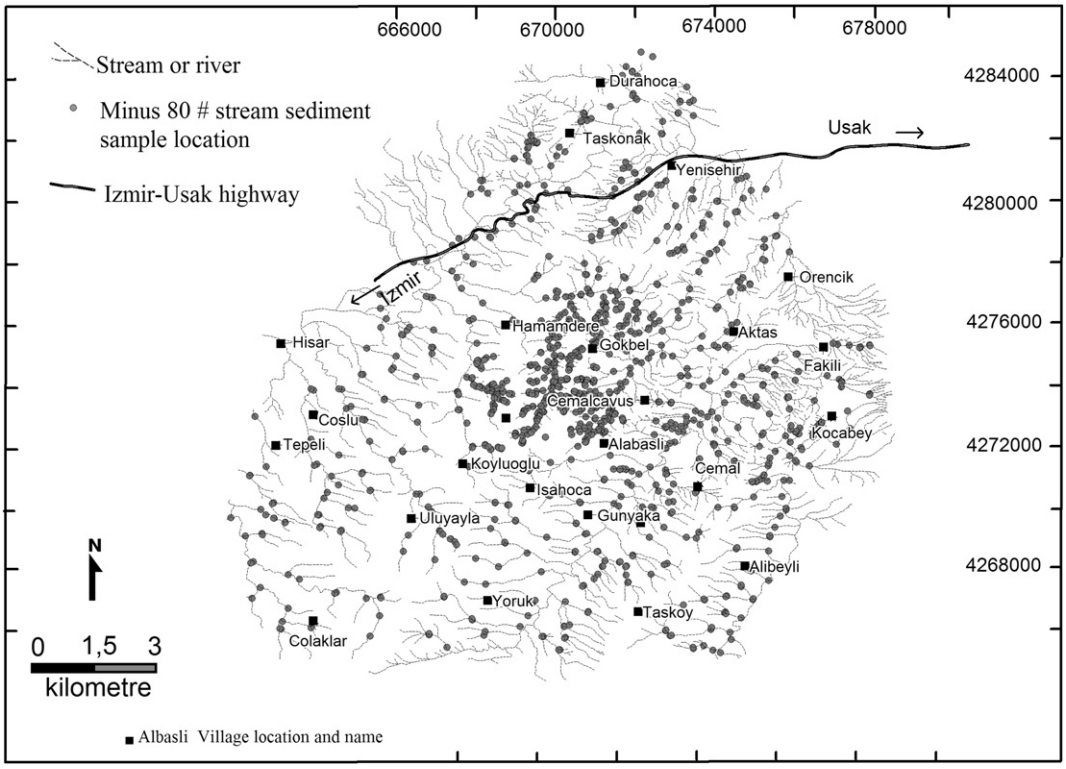

Fig. 6. Detailed −80 mesh stream sediment sampling survey in the Cemalcavus area.

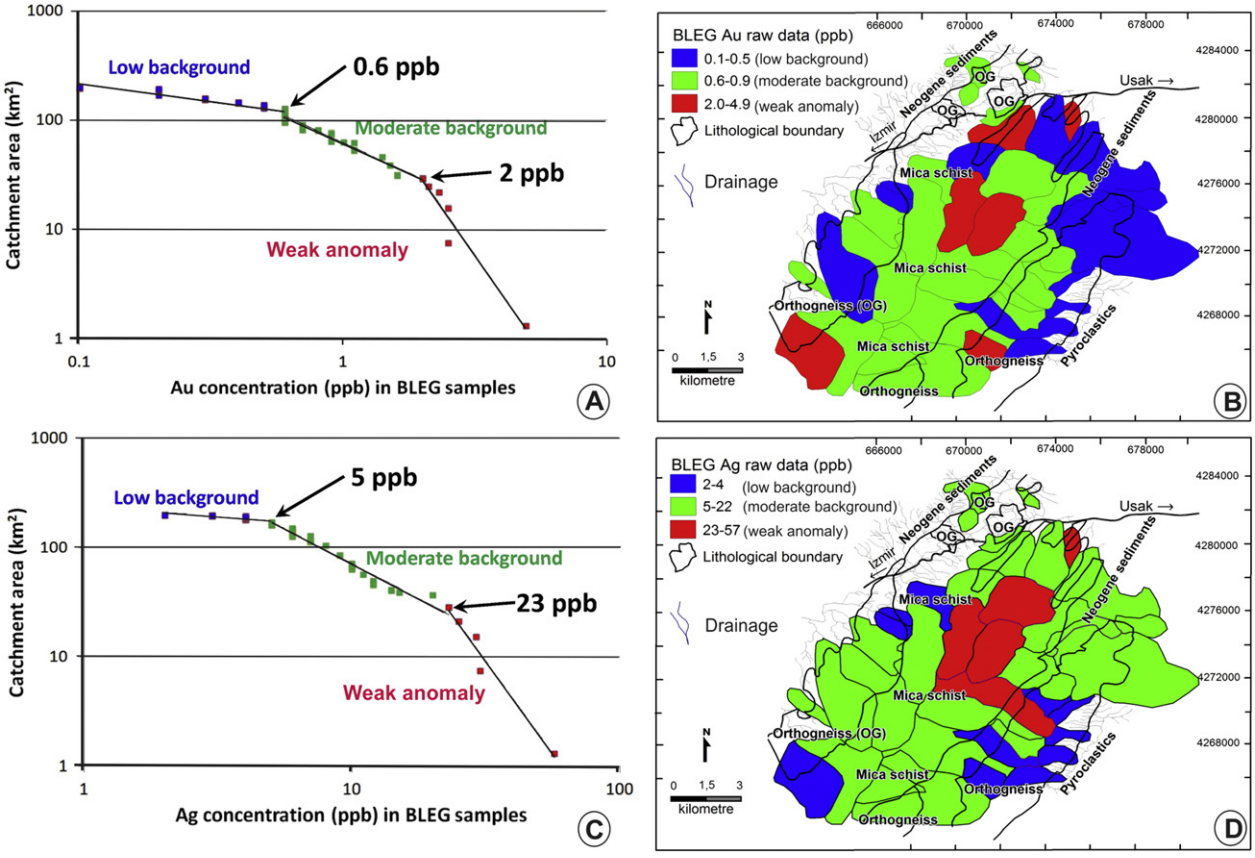

Fig. 7. Cemalcavus area (A) log–log plot of C–A model BLEG Au residuals, showing background (blue and green squares) and low anomaly populations in the data, (B) spatial distributions of background and anomalous populations of dilution-corrected Au residuals based on thresholds recognized in the C–A plot, (C) log–log plot of C–A model BLEG Ag residuals, showing background (blue and green squares) and low anomaly populations in the data and (D) spatial distributions of background and anomalous populations of dilution-corrected Ag residuals based on thresholds recognized in the C–A plot.

Table 1
Summary of statistical values for the −16 mesh BLEG stream sediment geochemical data set of the Cemalcavus area.

Elements	Au	Ag	Au	Ag
Data type	Raw data		Log10-antilog transformation	
N	40.00	40.00	40.00	40.00
Units	ppb	ppb	ppb	ppb
Detection limit	0.10	1.00	0.10	1.00
Minimum	0.10	2.00	0.10	2.00
Maximum	4.90	57.00	4.90	57.00
Mean	1.00	11.00	0.63	7.76
Median	0.60	7.00	0.60	7.08
SD	0.94	10.00	2.51	2.04
SD/Mean	0.90	0.63	3.88	0.26
MAD	0.68	6.68	0.68	6.68
Median + 2MAD	2.00	21.00	4.78	10.72
Q1	0.40	4.00	0.40	4.00
Q3	1.10	11.25	1.10	11.00
Skewness	2.40	3.00	0.70	6.00
Kurtosis	7.60	10.00	0.60	2.50

SD: Standard deviation, MAD: Mean of absolute deviation, Q1: First quartile, Q3: Third quartile, N: Number of samples.

deposits (Ercan et al., 1978). Quartz veins of metamorphic origin, ranging from a few centimeters to few meters in thickness, commonly occur as both cutting and parallel to schistosity planes of the metamorphic crystalline rocks, and are associated with hematite and limonite gossans. Two groups of normal faults with minor strike-slip components exist in the study area: (i) N30E-trending faults associated with strong phyllic alteration and E–W-striking epithermal quartz veinlets; and (ii) N60W-trending normal faults. Fractures associated with either of these normal faults are mostly filled with hematite–limonite–silica material reaching tens of centimeters in thickness. Maximum density of fracturing is estimated as 13 fractures per square meter.

In this study, a reconnaissance XRD alteration analysis, which has shown that the retrograde metamorphism initiated the mineral transformation from garnets or biotites to chlorites and from feldspars to sericite assemblage, also recognized two types of alterations, namely: (i) extensive sericite and chlorite, with local albite alteration (Fig. 3A, B) occurring both within N60W-trending normal fault zones and schistosity planes of quartz–feldspar–garnet–mica schist; and (ii) hematitic–limonitic–phyllic–silicic alteration (Fig. 3C) within N60W- and E–W-trending fractures and less commonly along shear planes. Phyllic alteration is represented by sericite indicating moderate temperature (min: 220 °C) of mineral formation (Fig. 2) and near-neutral conditions (Reyes, 1991; White and Hedenquist, 1995). The XRD study also identified kaolinite and montmorillonite within fault and fracture zones.

Two styles of mineralizations, which were discovered by the follow-up of Au anomalies defined by the BLEG, stream sediment and soil surveys discussed below, exhibit the following characteristics: (i) schistosity-conformable quartz–pyrite–arsenopyrite veinlets or breccias and disseminations with vug-infill, euhedral- and comb-quartz textures representing a deeper level of the epithermal system; and (ii) minor epithermal quartz veinlets (max. 20 cm wide) with Mn-oxide stains and crustiform, carbonate replacement and vug-in-fill textures cut schistosity planes, were found ~1.4 km ENE of Sarihasan (Fig. 2). Dark gray, schistosity-conformable, pyrite–arsenopyrite–Au–Ag or rare pyrite–arsenopyrite with minor galena–sphalerite–stibnite-rich quartz-vein breccias or veins (i.e., first mineralization style) of up to 3 m in thickness with 400 m strike length were found ~1 km S and SE of Cemalcavus (Figs. 2 and 3D–F). These multi-level mineralizations appear to be controlled by the schistosity or shear planes of the metamorphic schists and occur mainly as fracture fillings (Fig. 3F), crackle breccias, disseminations (Fig. 3G) and dendritic veinlets (Fig. 3H).

2.3. Climate and topography

The Esme area is dominated by a semi-arid climate with dry summers and cold and relatively wet winters. June, July and August are the hottest months with average temperatures of ~20 °C, whereas January and February are the coldest with temperatures of ~4 °C. Annual precipitation is 760 mm, mostly falling in winter and spring seasons. The topography in the Esme area is dominated by NE–SW, E–W and NW–SE–trending first-order river valleys, which are the surface expressions of NE–SW and E–W-trending graben structures. The landscape is generally smooth to gentle with elevations ranging from 500 m to 900 m. However, topography is rugged on the escarpment and local changes in elevation of 100–200 m occur within short distances, in particular around Hamamdere, Taskonak and Yenisehir (Fig. 4). Major drainages such as the E–W-flowing perennial Gediz River and the semi-perennial Kurbagali Stream flow within narrow grabens. However, a majority of the streams are ephemeral during summer. Stream sediment sampling was carried out in June–August in 2010, during a period of long sunny, rainless weather, so the stream flows remained low energy throughout the sampling program.

Hills in the Esme area are covered mainly by bushes. Cultivation is limited to grain and minor fruit because of lack of large fertile valleys. Visual examination has shown that organic matter content of stream sediments is very low and rarely moderately high. Stream slopes are generally gentle and rarely exceeds 25°. Weathering of the gneisses and schists is shallow, mainly less than 50 cm, with deeper weathering along faults. The stream sediments are composed mainly of quartz and feldspar with minor mica, non-degraded organic debris. Vegetation over the study area is dominated mainly by oak and shrub with minor willow developed along streamlines. Soil profile in the area is represented by B and C horizons with minor A horizon which was developed near permanent wet deep valleys.

(A)

Sample No	Au (ppb)	Ag (ppb)	Explanation
2583	2,3	25	Minus 16 mesh
2583.UP	11,4	69	Minus 80 mesh unpulverized
2583.PU	27,2	68	Minus 80 mesh pulverized
2580	2,5	30	Minus 16 mesh
2580.UP	6,6	54	Minus 80 mesh unpulverized
2580.PU	2,1	43	Minus 80 mesh pulverized
2586	0,6	6	Minus 16 mesh
2586.UP	0,9	9	Minus 80 mesh unpulverized
2586.PU	2	16	Minus 80 mesh pulverized
2599	2,5	4	Minus 16 mesh
2589.UP	4,2	8	Minus 80 mesh unpulverized
2589.PU	4,3	9	Minus 80 mesh pulverized
2571	0,9	5	Minus 16 mesh
2571.UP	1,8	10	Minus 80 mesh unpulverized
2571.PU	1,6	12	Minus 80 mesh pulverized

(B)

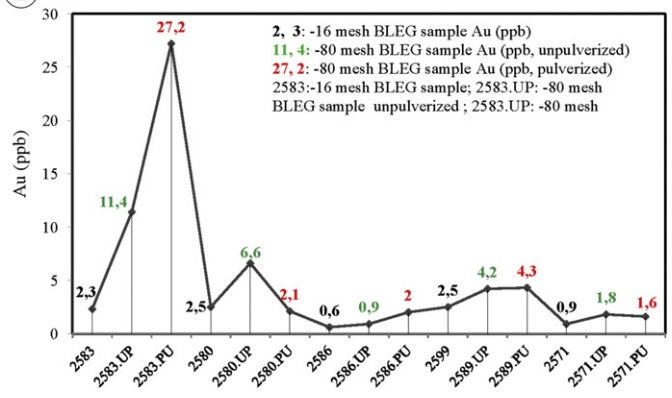

Fig. 8. Variation of Au contents in (A) tabulated −16 and both unpulverized and pulverized −80 mesh BLEG stream sediment samples, and (B) graphical presentation BLEG Au contents in −16 and −80 mesh stream sediment samples.

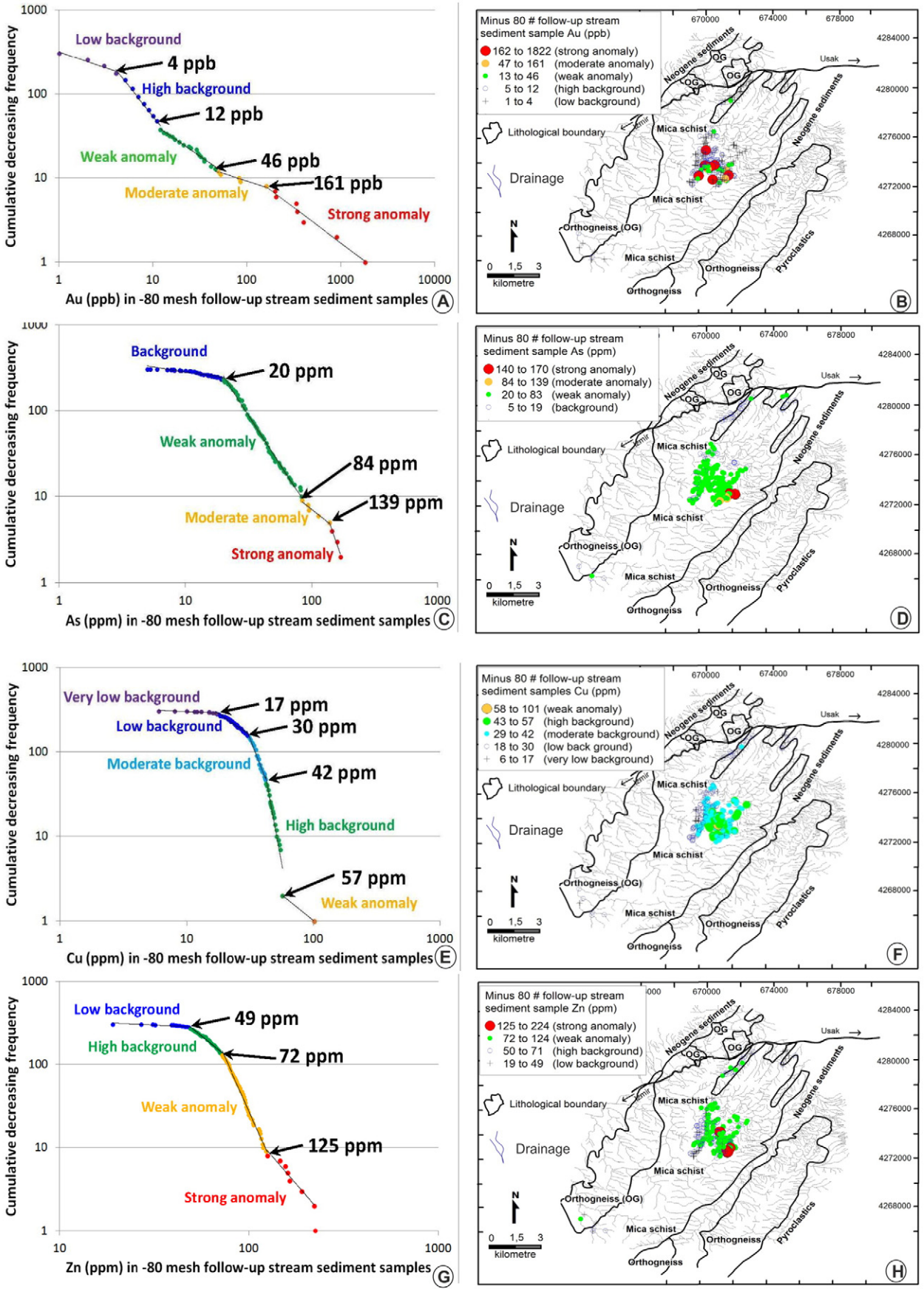

Fig. 9. Log–log plots of −80 mesh BLEG fallow up (C–A method) for: (A) Au, (C) As, (E) Cu and (G) Zn, and geochemical population distribution maps for: (B) Au, (D) As, (F) Cu and (H) Zn based on C–A method.

3. Geochemical sampling and geo-analysis

The precision of geo-analyses for all sample types was better than 10% at the 95% confidence level using the method of Thompson and Howarth (1978).

3.1. Sampling for BLEG (bulk leach extractable gold) geo-analysis

Stream sediment sample locations for BLEG analysis were defined from published 1:25.000 scale topographic maps to reach a sample density of approximately one sample per 5 km^2 (Fig. 4). However, a homogeneous distribution of samples was not feasible due to poor access by vehicle in many parts of the study area (Fig. 4). Each sampling site was selected so that, if applicable, it was far enough upstream from any higher-order stream to minimize the influx of sediment from the larger stream. Sampling was not carried out within 100–150 m of human habitation. A team consisting of one geologist and one sampler was able collect an average of seven samples per day. Active silt- to sand-size, generally wet stream sediments weighing 3–6 kg were collected along some 20–60 m of the stream to produce 2 kg of −16 mesh fraction for BLEG analysis after sieving. Wet or moist samples were first dried in oven at 90 °C prior to sieving. It should be emphasized with confidence that due to excessive care no potential loss of colloidal or organic-adsorbed, if any, Au through sieving during dry-screening of sediments in the laboratory. In total, 40 BLEG samples were collected to cover the study area.

In the laboratory, samples for BLEG (−16 mesh) analyses were leached in 2 l of cyanide solution in a bottle roller, tumbler, with 0.1–0.3% cyanide and either lime or sodium hydroxide, and rolled for 12 h (Yilmaz, 2003). The efficiency for extraction was dependent on cyanide concentration as well as pH, oxygen being available, duration of agitation, particle size, availability of gold and the absence of competing precipitants for gold, for example, organic matter, sulfides, etc. (cf. Beeson, 1995; Mazzucchelli, 1990). The metals, which were leached in 2 l of cyanide solution, were precipitated on zinc powder. Zinc is normally re-dissolved in acid to re-solubilize gold. The zinc concentrates were filtered from solution and then measured for Au and Ag by AAS (atomic absorption spectrometry).

3.2. Minus 80 mesh stream sediment sampling and geo-analysis

In order to determine the most suitable grain-size ranges for stream sediment Au analysis, eight samples were collected from immediately south of Cemalcavus, where distinct sericitic–chloritic alteration encompasses arsenopyrite-bearing silicified mica schists. These samples were further sieved into three grain size fractions using aluminum-bodied sieves with −16 mesh + 42 mesh, −42 mesh + 80 mesh, and −80 mesh sizes. Each fraction of the stream sediment was sent for analysis for assay of Au and by ICP-ES for 49 elements including Ag, Cu, Pb, Zn, As, Sb and Mo following a HNO_3/ $HClO_4$ digestion in ALS laboratories. The geochemical contrast for Au was greatest in the −80 mesh fraction (Fig. 5).

BLEG stream sediment samples returning Au values above 2 ppb were followed up with −80 mesh stream sediment sampling (Fig. 6). Two drainage catchments that are located among Hamamdere–Sarıhasan–Albaslı–Cemalcavus–Gokbel were −80 mesh sampled at high density (16 samples/km^2) due to recognition of intense sericite–chlorite alteration whereas remaining drainage catchments were −80 mesh sampled at low density (4 samples/km^2) due to lack of any significant alteration. Some 308–80 mesh BLEG follow-up stream sediment samples were collected from the study area.

The study area was blanket-covered with −80 mesh stream sediment sampling of drainages returning BLEG Au of <2 ppb for comparison with the efficiency of BLEG sampling to detect anomalies of Au and Ag as well as other elements (Fig. 6). A total of 741–80 mesh stream sediment samples were collected during blanket coverage stage of the area. The sampling density for the second −80 mesh stream sediment survey was varied from 3 to 5 samples per square kilometer (Fig. 6). In both stream sediment sampling campaigns, mainly clay- and silt-size stream sediments were sampled along 20–30 m section of an active stream, upstream from a junction. Where the stream sediments were too wet to sieve, a bulk sample was collected for later drying and sieving; in case of dry streams, sediments were sieved on-site to provide 500 g of the −80 mesh fraction for analysis.

In the laboratory, the stream sediment samples were analyzed by ICP-ES for 49 elements including Ag, Cu, Pb, Zn, As, Sb and Mo following a HNO_3/ $HClO_4$ digestion. Gold was determined by GFAAS at ALS after a 3:2:4 HCl/ HNO_3/HF attack and dissolution with HBr followed by uptake in MIBK (Fletcher and Horskey, 1988; Meier, 1980).

3.3. Soil sampling and geo-analysis

BLEG and stream sediment anomalies were followed-up with −80 mesh soil sampling for conventional (from B-horizon) and MMI (from 10–20 cm below the surface) geochemical analysis. An initial conventional soil sampling grid with WNW orientation was designed taking into account major NE-trending regional structures and the −80 mesh stream sediment anomalies, which were clustered around Koca Tepe. Some 546 conventional soil samples were collected to cover an area of about 2.5 km^2. At this initial stage with associated prospect-scale mapping, W- to NW-trending fractures filled with quartz–hematite veinlets were recognized. Therefore, the orientation

Table 2
Summary of statistical values for the −80 mesh all stream sediment geochemical data set of the Cemalcavus area.

Elements	Au	Ag	Cu	Pb	Zn	As	Sb	Au	Ag	Cu	Pb	Zn	As	Sb
Data type	Raw data							Log10-antilog transformation						
N	1049	630	1049	1049	1049	1049	630	1049	1049	1049	1049	1049	1049	630
Units	ppb	ppm	ppm	ppm	ppm	ppm	ppm	ppb	ppm	ppm	ppm	ppm	ppm	ppm
Detection limit	1	0.01	0.2	0.5	2	0.2	0.05	1	0.01	0.2	0.5	2	0.2	0.05
Minimum	1	0.01	2	4	16	4	0.2	1	0.01	2	4	16	4	0.2
Maximum	1815	0.66	101	417	224	335	115	1815	0.66	101	417	224	335	115
Mean	9	0.08	26	16	63	22	2.8	2.6	0.06	25	16	58	17	1
Median	2	0.07	24	16	59	16	1.0	2	0.06	25	16	58	16	1
SD	68	0.06	11	14	26	24	7.0	3.2	2	2	2	2	2	3
SD/Mean	7.5	0.75	0.42	0.87	0.41	1.1	2.5	1.23	33.33	0.08	0.16	0.03	0.12	3
MAD	12	0.04	9	4	19	11	2.9	2	1.78	2	2	2	2	2
Median + 2MAD	26	0.15	42	24	97	38	6.8	6	3.66	29	20	62	20	5
Q1	1	0.04	17	13	46	11	0.7	1	0.04	17	13	46	11	0.70
Q3	4	0.1	33	19	77	26	2.1	4	0.10	33	19	78	26	2.10
Skewness	20	4	1	25	2	6	10	63	0.32	0.2	3	1	4	0.00
Kurtosis	497	25	2	729	5	47	132	79,432	3.16	13	50,118	2	19	25

SD: Standard deviation, MAD: Mean of absolute deviation Q1 and Q3: First and third quartiles N: Number of samples.

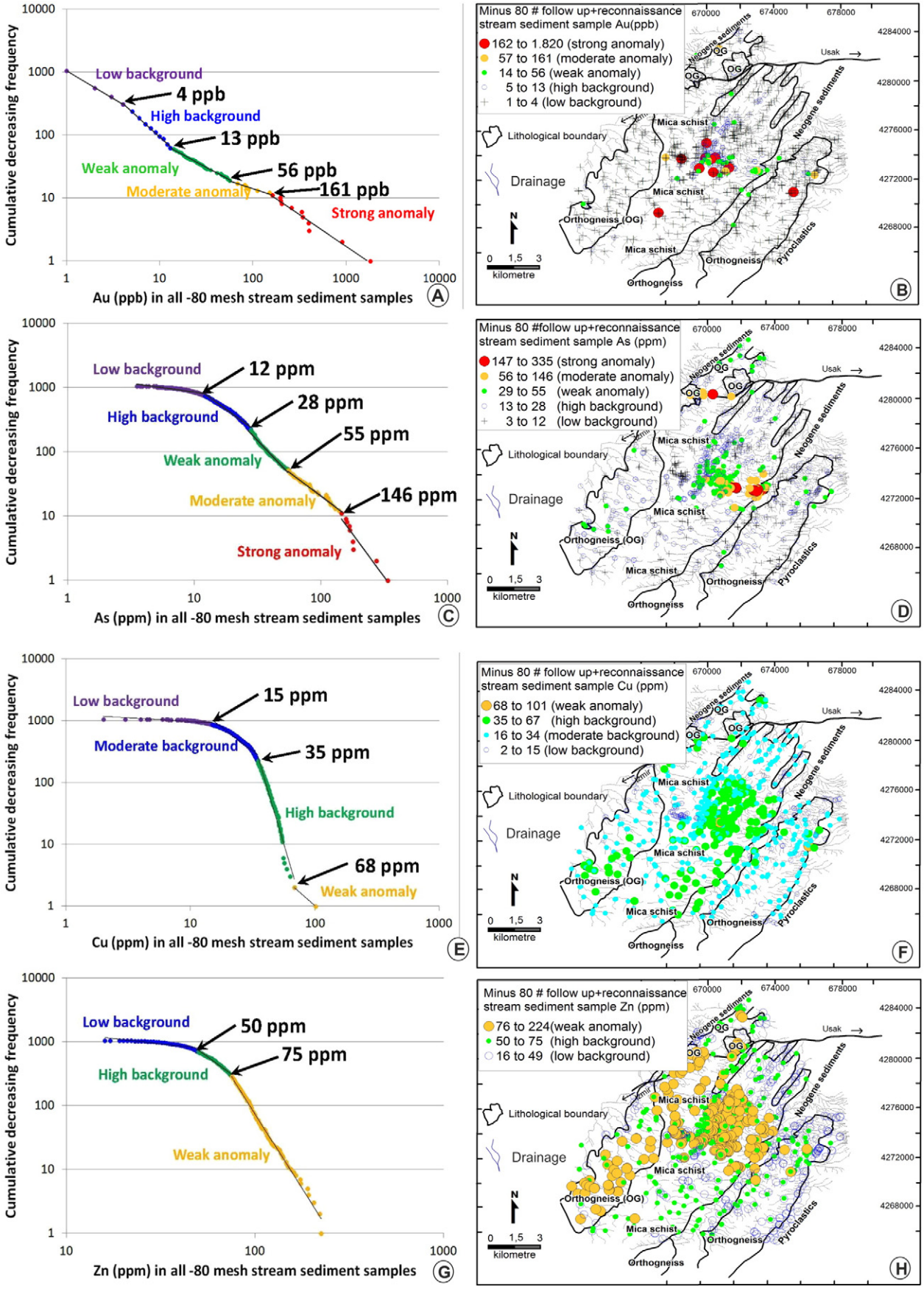

Fig. 10. Log–log plots of all-80 mesh BLEG fallow up and blanket coverage (C–A method) for: (A) Au, (C) As, (E) Cu and (G) Zn, and geochemical population distribution maps for: (B) Au, (D) As, (F) Cu and (H) Zn based on C–A method.

of both conventional and MMI soil sampling grid was re-designed to be perpendicular or semi-perpendicular so as to cut these fractures. A total of 640 second stage conventional soil samples covering 3 km^2 were collected. Soil samples for conventional soil analysis were sent to ALS laboratories for assay of Au and 51 other trace elements by Au-ICP21 and ME-MS41 methods, respectively. Soil samples for MMI analysis were also sent to ALS laboratories for measurements of 62 elements including Au and Ag by the method ME-MS23 method.

The MMI analysis enables detection of buried mineralization using surface soil, through dissolution and subsequent measurement of weakly bound ions loosely attached to surface particles. The ability of this leach to get close to true background detection limits makes it effective in providing geochemical contrast and targeting buried mineralization (Mann et al., 1998, 2005). In sample preparation for MMI analysis, the sodium cyanide leach is buffered to pH 8.5 using EDTA (ethylene diamine tetra-acetic acid) to liberate weakly bound ions from particle surfaces. The leach is carried out on a 50 g aliquot of −80 mesh fraction. Samples are agitated every two hours for six hours at 21 °C. The final solution is centrifuged and the fluid decanted for analysis of 62 elements by the ME-MS23 method (ALS minerals booklet, schedule of services and fees, 2012). Therefore, the sample preparation for the MMI soil analysis represents partial extraction, which is quite different from the almost-total extraction conventional soil analysis.

4. Geochemical data analysis

Average trace-element contents of metamorphic rocks (aqua regia digestion/ppm) are: 0.005–0.006 for Au, 0.06–0.1 for Ag, 10–30 for Cu, 0.1 for Pb, 50 for Zn, 1 for As, 0.1 for Sb (Beus and Grigorian, 1977), 0.3 for Mo, 0.1–0.5 for W or Bi (Taylor, 1966). Average concentrations (ppm) for these elements in soil are also reported by Levinson (1974) as: 0.1 for Ag, 2–100 for Cu, 2–200 for Pb, 10–300 for Zn, 1–50 for As, 5 for Sb, 2 for Mo and no data for Au and Bi. Stream sediment and soil background values have been commonly determined as the mean and median values of lognormal distributions (Rose et al., 1979; Xueqiu et al., 1999) whereas the median of lognormal distribution is suggested as the background by Levinson (1974) until late in 19th century. Statistical models can be applicable to sample populations with normal distribution but are not applicable when sample populations display positive or negative skewness. The *median + 2MAD* statistical technique of exploratory data analysis (EDA) has been extensively used to differentiate geochemical anomalies from background (Asadi et al., 2013; Carranza, 2009; Reimann and Garrett, 2005). The *MAD* is estimated as the median of absolute deviations of all data values from the data median (Tukey, 1977). Hypothesis generation is the chief objective of EDA and it overcomes the non-normality limitation by generating potentially explainable data patterns. Recently, however, stream sediment background determinations were done by fractal analysis, which is claimed to be more robust than *median + 2MAD* and *mean + 2SD* (Afzal et al., 2010; Carranza, 2010; Arias et al., 2012; Goncalves et al., 2001; Hao et al., 2014; Li et al., 2003; Luz et al., 2014). Cheng et al. (1994) proposed the concentration–area (C–A) fractal model that was used here to distinguish the geochemical anomalies and background. Carranza (2010) has demonstrated that, in mapping of stream sediment anomalies, the C–A fractal method outperformed the *median + 2MAD* and *mean + 2SD* methods of identifying the threshold values. The concept of C–A fractal method was summarized by Carranza (2010) as follows: "in a study area, geochemical concentration levels (v) and the cumulative areas (A) enclosed by each geochemical concentration level (i.e., $A(v)$) are plotted along the x-axis and y-axis, respectively, on a log–log graph. A C–A plot describes not only the empirical frequency distributions of geochemical concentration levels but also the spatial distributions and geometrical properties of the features defined by different geochemical concentration levels. Concentration–area plots invariably satisfy certain power-law functions, which are depicted as straight lines (or line segments) on a log–log graph. If a C–A plot can be depicted by one straight-line then it probably represents a fractal distribution of geochemical background. If, on the other hand, a C–A plot can be depicted by at least two straight-line segments, then the rightmost straight-line segment (i.e., highest concentration values) probably represents a fractal distribution of geochemical anomalies, whereas the straight-line segment(s) to the left probably represent(s) a multifractal distribution (or inter-twined fractal distributions) of geochemical background. Accordingly, the breaks in slopes of straight-line segments fitted through a log–log plot of the C–A relationship represent threshold values of different ranges or populations of concentration values in a geochemical data set. These different populations would represent different background and anomalous geochemical processes, one of which could be mineralization".

The separation between background and anomalous values in BLEG and −80 mesh conventional stream sediment geochemical data as well as conventional and MMI soil geochemical data in this study was defined by through C–A fractal modeling, and line segments were fitted to the generated C–A log–log plots. Values corresponding to breaks between straight-line segments have been used as threshold values separating various populations, which are interpreted as levels (weak, moderate strong) of either background or anomalies of Au, As, Cu and Zn. A combination of Excel-2007, Surfer-12 and Mapinfo Professional soft ware was used for statistical analysis and plotting.

4.1. Analysis of BLEG stream sediment data

Threshold BLEG Au and Ag values were defined by using C–A fractal analysis, which generated six Au and five Ag BLEG anomalies (Figs. 4

Table 3
Summary of statistical values for the −80 mesh soil geochemical data set of the Cemalcavus area.

Elements	Au	Ag	Cu	Pb	Zn	As	Au	Ag	Cu	Pb	Zn	As
Data type	Raw data						Log10-antilog transformation					
N	1186	1186	1186	1186	1186	1186	1186	1186	1186	1186	1186	1186
Units	ppb	ppm	ppm	ppm	ppm	ppm	ppb	ppm	ppm	ppm	ppm	ppm
Detection limit	1	0.01	0.2	0.2	2	0.05	1	0.01	0.2	0.2	2	0.05
Minimum	1	0.03	3	4	30	5	1	0.03	3	4	30	5
Maximum	488	4.40	357	1950	520	594	488	4.40	357	1950	520	594
Mean	11	0.38	39	17	84	38	5	0.25	28	13	79	28
Median	5	0.50	35	13	79	26	5	0.24	26	13	79	26
SD	29	0.33	23	71	36	36	3	2.15	2	2	1	2
SD/Mean	2.6	0.86	0.59	4.2	0.4	0.95	0.6	8.60	0.07	0.15	0.01	0.07
MAD	10	0.21	27	10	22	27	2	2.00	2	1	1	2
Q1	2	0.15	28	9	67	19	2	0.13	28	9	68	19
Q3	5	0.60	35	13	79	26	5	0.24	35	13	79	26
Skewness	11	5.30	5	24	4	6	3	0.95	0	60	7	10
Kurtosis	146	49.00	48	612	33	42	3	0.42	2692	15,135	2089	158

SD: Standard deviation, MAD: Mean of absolute deviation, Q1 and Q3: First and third quartiles, N: Number of samples.

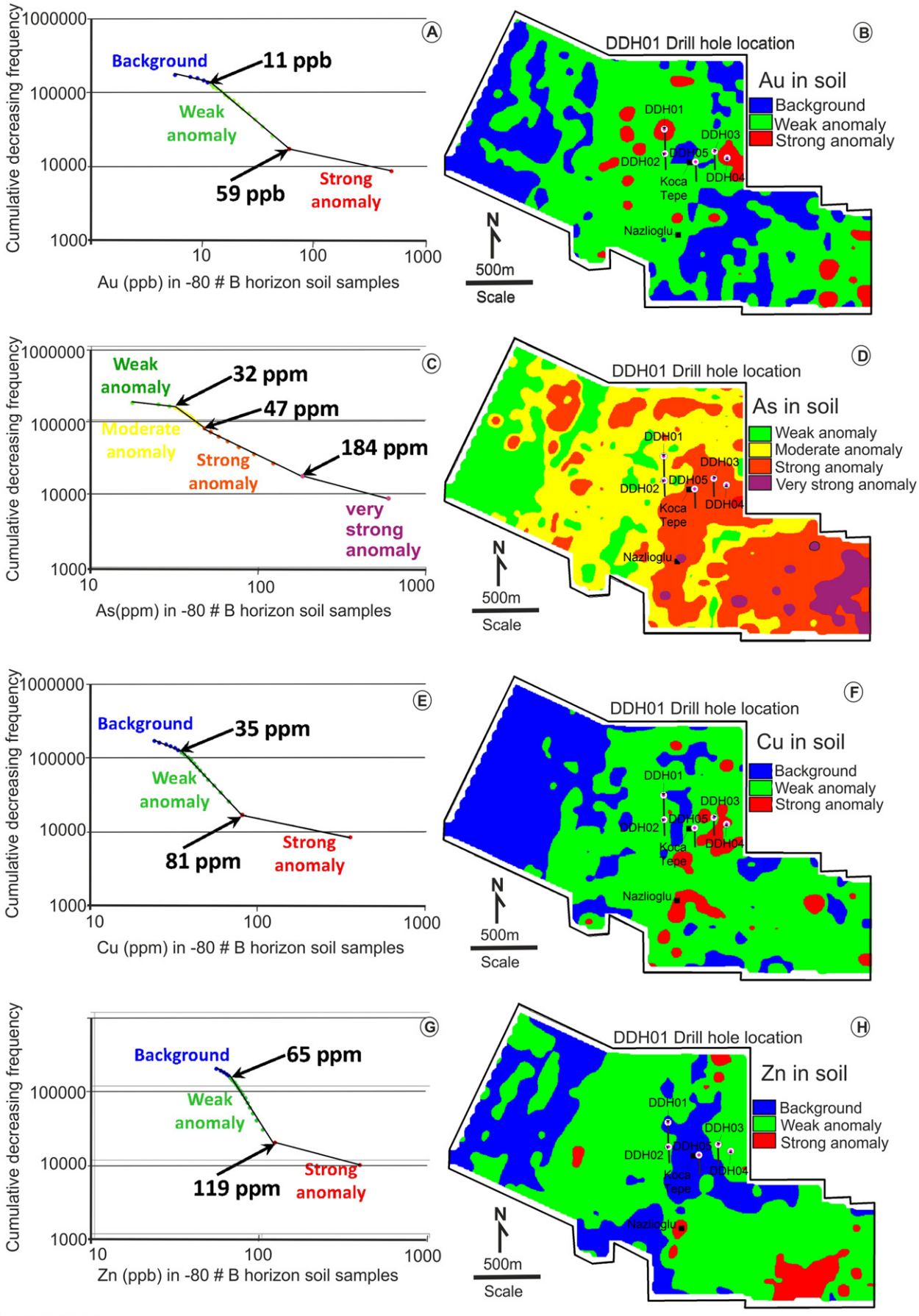

Fig. 11. Log–log plots of conventional soil (C–A method) for: (A) Au, (C) As, (E) Cu and (G) Zn, and maps showing the spatial distribution for: (B) Au, (D) As, (F) Cu and (H) Zn based on C–A method.

and 7). The statistical parameters of data for these elements are shown in Table 1. As indicated by the data, all distributions are positively skewed (for raw and log data) whereas kurtosis are ≫0 indicating too much peak. Therefore, classical statistical models such as *mean + 2SD* or *median + 2SD* data treatment are not applicable to the BLEG data. Regional BLEG stream sediment anomalies ranged from 2.0 ppb to 4.9 ppb Au (Table 1), and these values were obtained from 1.7 km E of Yenisehir, 2 km N and E of Gokbel and 2.5 km NW of Colaklar (Figs. 4 and 7A, B). An alternative method of −80 mesh BLEG sampling was tested for Au and Ag responses by collecting five samples from the former five BLEG sample locations. Although the classical statistical methods were not applicable due to insufficient number of samples, Au and Ag values of −80 mesh BLEG stream sediment increased three to five fold as compared to those of −16 mesh samples (Fig. 8). In other words, −16 mesh and −80 mesh BLEG samples, which were collected from a stream catchment immediately west of Gokbel, returned 2.3 ppb and 11.6 ppb (unpulverized) Au values, respectively, with the latter yielding a 5-fold Au value compared to the former. The Colakalar (2.5 ppb Au) and Yenişehir (4.9 ppb) Au anomalies may have been due to contamination caused by villages located within the drainage basins because −80 mesh follow-up stream sediment sampling (Figs. 7 and 9) and geology mapping yielded no anomalous Au values (≤8 ppb Au at Colaklar and ≤4 ppb Au at Yenisehir) and noticeable alteration, respectively.

4.2. Analysis of −80 mesh stream sediment geochemical data

The statistical parameters of elements from the BLEG follow-up and reconnaissance blanket coverage −80 mesh stream sediment sampling are shown in Table 2. Data from Table 2 indicate that all distributions are positively skewed (for raw and log data) except for not skewed or slightly skewed Ag, Cu and Sb. Kurtosis are ≫0 indicating too much peak. The raw and log-transformed Au data display the largest skewness as compared to other associated elements. Therefore, classical statistical models such as *mean + 2SD* or *median + 2SD* data treatment are not applicable to the −80 mesh stream sediment data. The separation between the background and anomalous Au, As, Cu and Zn values was defined by using fractal C–A model (Fig. 9). BLEG follow-up −80 mesh stream sediment sampling resulted in the recognition of several moderate to strong Au and As anomalies within the Cemalcavus area (Figs. 9). Au and As values ranged up to 1815 ppb and 335 ppm, respectively. Only 12 of the original Au values being classified as moderate to strong anomalies are greater than 47 ppb whereas eight of the original As values, which are higher than 85 ppm, are assigned to moderate to strong anomalies in BLEG follow up stream sediment samples. Au is spatially associated with As (Fig. 9A–D). For the strong anomalies, −80 mesh follow stream sediment samples returned seven Au and four As strong anomalies. Cu returned only one weak anomaly (101 ppm) whereas a larger number of weak to strong Zn anomalies (129 samples with ≥57 ppm) were generated. However, only eight strong Zn anomalies returned from −80 mesh follow-up stream sediment sampling. Copper shows a weak spatial association with Zn (Fig. 9E–H).

BLEG follow-up and reconnaissance blanket coverage −80 mesh stream sediment sampling yielded 12 moderate and 10 strong Au anomalies (Fig. 10A–D) and 24 moderate and 11 strong As anomalies (Fig. 10E–H) within the Cemalcavus area. Gold and As values ranged up to 1815 ppb and 335 ppm, respectively. Only 22 of the original Au values being classified as moderate to strong anomalies are greater than 56 ppb whereas 24 of the original As values are greater than 84 ppm in moderate and strong anomaly category. Au exhibits spatial association with As only in the central part, which is underlain by mica schist (Fig. 10A–D). The number of moderate to strong Au and As anomalies corresponds to about 2.1% of the total −80 mesh samples collected from the study area. Copper yielded only two weak anomalies (68 and 101 ppm) whereas several weak Zn anomalies (272 samples with ≥76 ppm), which were mainly confined to mica schist, were generated (Fig. 10E–H).

4.3. Analysis of soil geochemical data

In order to follow-up the −80 mesh stream sediment anomalies in the Cemalcavus area, −80 mesh conventional B-zone (4.2 km^2) and MMI (2.5 km^2) soil surveys were carried out at a line spacing of 100 m with samples at 50 m along lines.

The −80 mesh conventional soil samples contained values ranging from < 1 to 488 ppb Au, <0.03 to 4.4 ppm Ag, 3–357 ppm Cu, 4–1950 ppm Pb, 30–520 ppm Zn and 5–594 ppm As (Table 3). Data from Table 3 indicate that all distributions are positively skewed (for raw and log data) except for not skewed or normally distributed Cu with log data. Thus, soil data could not be assessed using classical statistical models due to positive skewness. The conventional soil data, therefore, was analyzed using the C–A fractal model to set threshold values for defining classes of uni-element soil background and anomalies for Au, As, Cu and Zn (Fig. 11A–H). About 29 of the conventional Au values are greater than 59 ppb whereas 46 and 97 of conventional Cu and Zn values, which are classified as strong anomalies, are greater than 80

Table 4
Summary of statistical values for the MMI soil geochemical data set of the Cemalcavus area.

Elements	Au	Ag	Cu	Pb	Zn	As	Au	Ag	Cu	Pb	Zn	As
Data type	Raw data						Response ratios (RR)					
Units	ppb	ppb	ppb	ppb	ppb	ppb	RR	RR	RR	RR	RR	RR
N	949	949	949	949	949	949	949	949	949	949	949	949
Detection limit	0.02	0.1	1	1	10	2	0.02	0.1	1	1	10	2
Data type	Raw data						Response ratios (RR)					
Minimum	0.1	3	66	1	10	2	1	1	1	1.0	1	1
Maximum	63.7	785	8920	209	1020	157	159	59	28	77.0	10	43
Mean	2.7	49	729	15	77	12	6.8	3.6	2.3	5.4	2.2	3.0
Median	1.4	30	569	9	50	9	3.5	2.2	1.8	3.3	1.7	2.0
SD	4.7	65	593	19	87	14	11.7	4.7	1.9	6.9	1.5	4.0
SD/Mean	1.74	1.32	0.81	1.26	1.12	1.16	1.6	1.3	0.8	1.3	0.7	1.3
MAD	2.36	35	357	11	49	8	5.9	2.5	1.1	4.2	1.1	2.1
Median + 2MAD	6	100	1283	31	148	25	15.3	4.7	4.0	11.7	3.9	4.1
Q1	0.7	19	410	4	40	5	1.7	1.4	1.3	1.5	1.0	1.0
Q3	3	54	855	17	90	14	7.5	4.0	3.0	5.0	3.0	2.0
Skewness	6.1	5	5	5	5	5	6.2	5.6	5.0	5.0	5.0	5.0
Kurtosis	55	40	46	36	30	34	55.2	44.5	48.0	36.0	30.0	34.0

SD: Standard deviation, MAD: Mean of absolute deviation, Q1 and Q3: First and third quartiles, N: Number of samples.

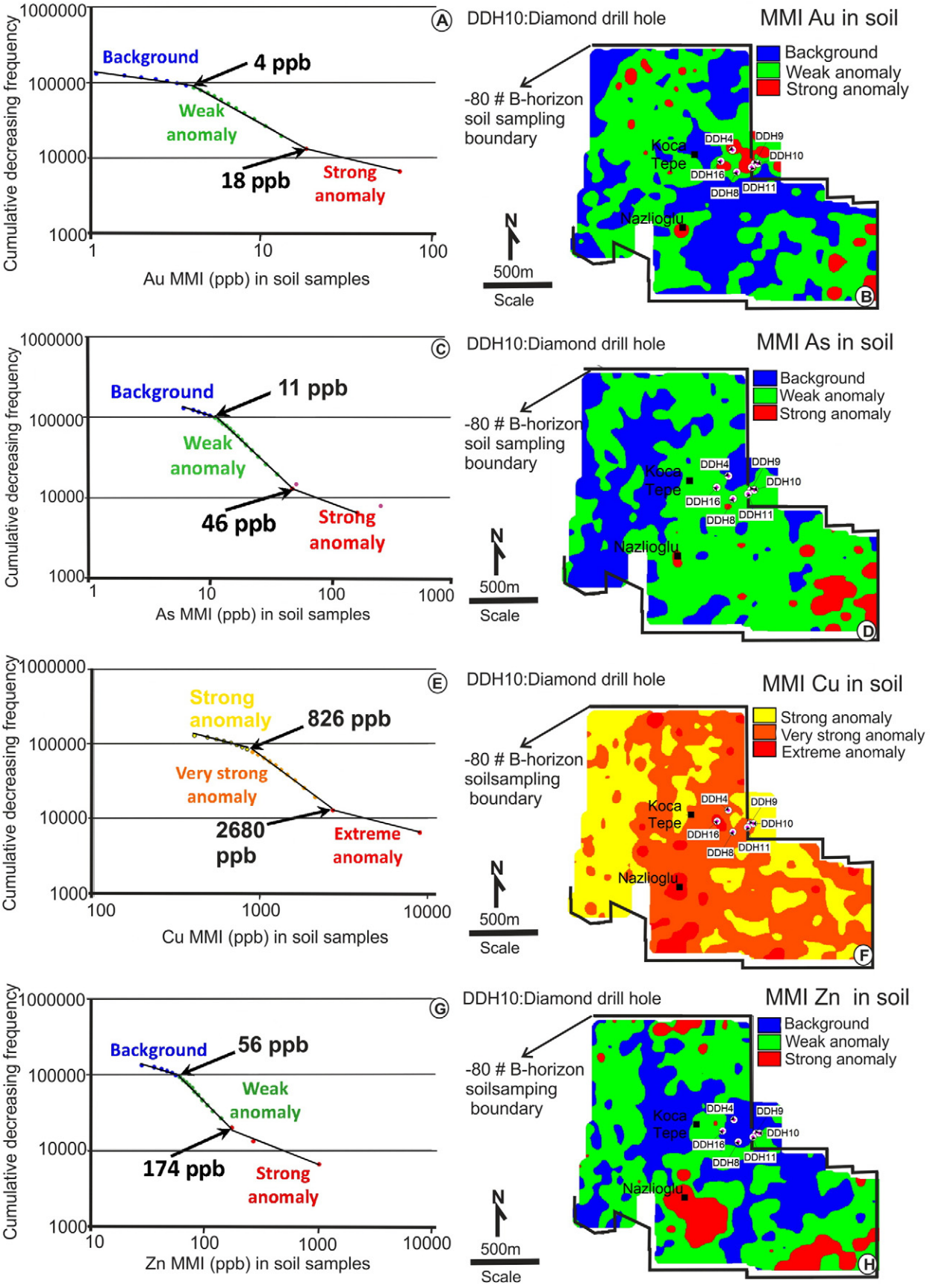

Fig. 12. Log–log plots of MMI soil (C–A method) for: (A) Au, (C) As, (E) Cu and (G) Zn, and maps showing the spatial distribution for: (B) Au, (D) As, (F) Cu and (H) Zn based on C–A method.

and 119 ppm, respectively. Importantly, 191 of conventional As values, classified as strong to very strong, are higher than 184 ppm.

MMI soil samples returned values ranging from < 0,1 to 63 ppb Au, <3 to 785 ppb Ag, 66–8926 ppb Cu, 1–209 ppb Pb, 10–1020 ppb Zn and <2–157 ppb As (Table 4). Data from Table 3 indicate that all distributions are positively skewed (for raw and log data). Like the conventional B-zone soil data, MMI soil data were analyzed using the C–A fractal model to set threshold values for defining classes of uni-element soil background and anomalies (Fig. 11A–H). About 89 of the MMI Au values > 4 and <17 ppb fall in the weak anomaly field whereas 18 of them with >17 ppb take place in strong anomaly area. Areal plots of Au, As, Cu and Zn anomalies are presented in Fig. 11A, C, E and G. Some 294 weak As anomalies (>55 and <174 ppb) are recorded over a large area whereas a smaller number of strong As anomalies occur in the southeast. Probably, the largest number weak Zn anomalies (475 with >55 ppb) occur almost over the whole area whereas smaller number of strong Zn anomalies (64 with >174 ppb) are located mainly in the south and southeast ends with minor strong Zn anomalies located at the north end (Fig. 11H). MMI Cu soil samples returned the largest number anomalies ranging from strong (<826 ppb) to very strong (826–2679 ppb) to extremely strong (2679–8920 ppb). In other words, the whole MMI soil sampling area is underlain by strong to extremely strong MMI Cu anomalies (Fig. 11F).

The threshold values for AuRR and AgRR were plotted for *median + 2MAD* and (Fig. 13A–D). When Fig. 12A with raw data is compared to Fig. 13A with RR data, Au anomalies in the latter appear to be more coherent than the former. Three roughly NE-trending coherent soil AuRR anomalies defined by 15RR for *median + 2MAD* (Fig. 13A) are centered at 672450 N/4273880E (165 × 370 m, far-NW), 673350 N/4273350E (350 × 3750 m, Koca Tepe-E) and 674100 N/4272420E (170 × 3550 m, Albasli-NE). Gold exhibits strong spatial overlap with Ag at the Koca Tepe-E (Fig. 13B) for *median + 2MAD* raw data.

5. Exploration drilling

Core samples of DDH01 and DDH02 from Phase I drilling returned no significant Au values in spite of the presence of partly underlying conventional coherent soil anomaly (Fig. 14). However, moderate IP/resistivity anomalies underlie the DDH01–DDH5 drill holes except DDH04, which is associated only with magnetite-destruction halo. The core samples from DDH03 returned Au values ranging from 100 to 670 ppb with depths ranging from 7 m to 90 m whereas the core samples from DDH05 yielded Au contents ranging from 150 to 670 ppb at depths of 60 to 215 m (Fig. 14, Table 5).

Conventional soil Au anomaly overlaps the MMI soil Au anomaly at the DDH04 location where very weak one meter-thick gold mineralization (130 ppb Au) was intersected at 20 m depth (Fig. 16). The remaining mineralization at depths of 22, 44, 78, 197 and 212 m yielded 130, 200, 170, 700 and 810 ppb Au, respectively (Figs. 15B and 16). Other MMI bulls-eye MMI soil anomalies were also tested by diamond drill holes DDH08, DDH09, DDH10, DDH11 and DDH16 (Phase II drilling) that gave rise to the discovery of schistosity-controlled Au mineralized

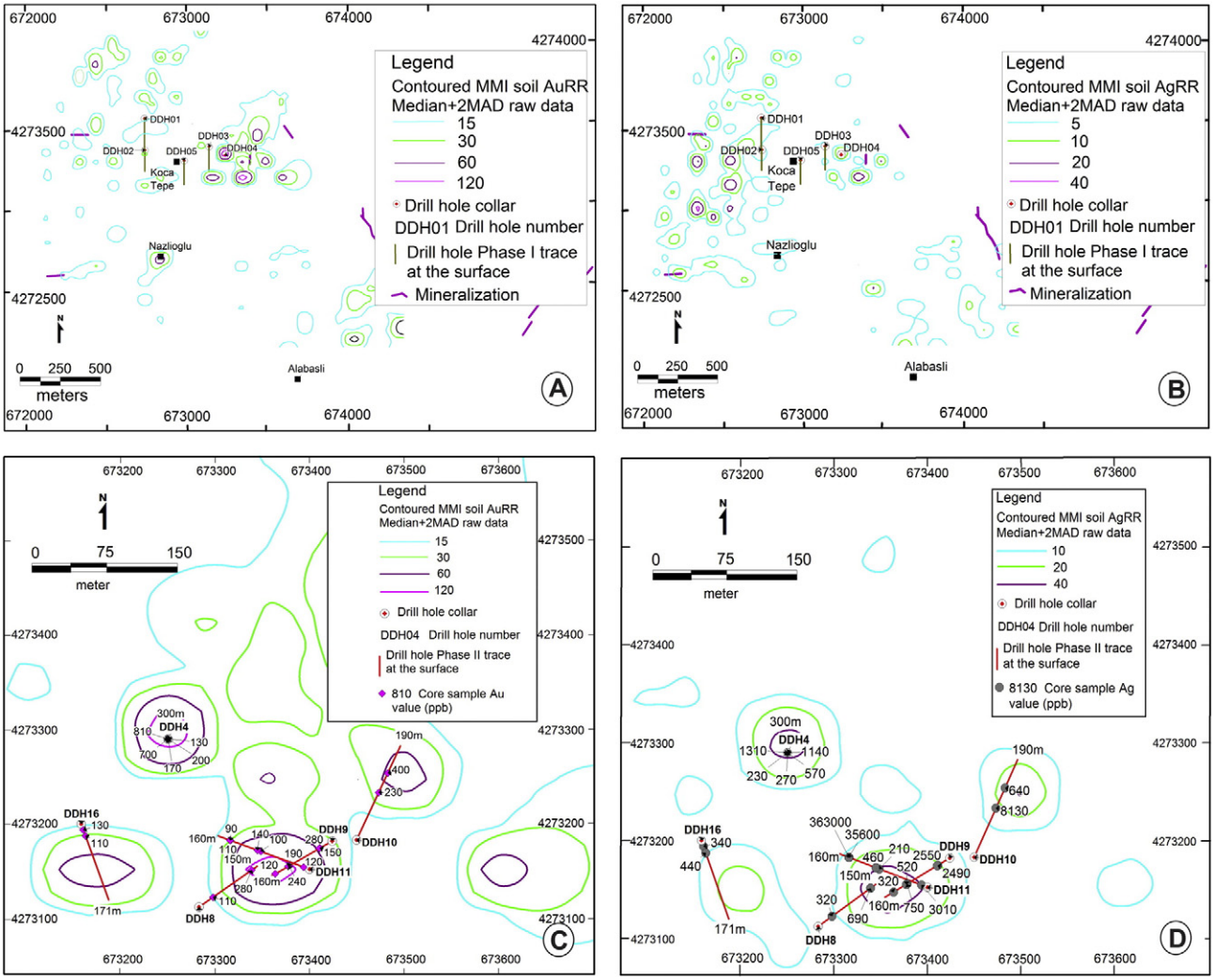

Fig. 13. Contoured MMI response ratio (median + 2MAD raw data) for: (A) Au and (B) Ag at Cemalcavus area, showing relation between MMI anomalies and drill-hole Au and Ag grades.

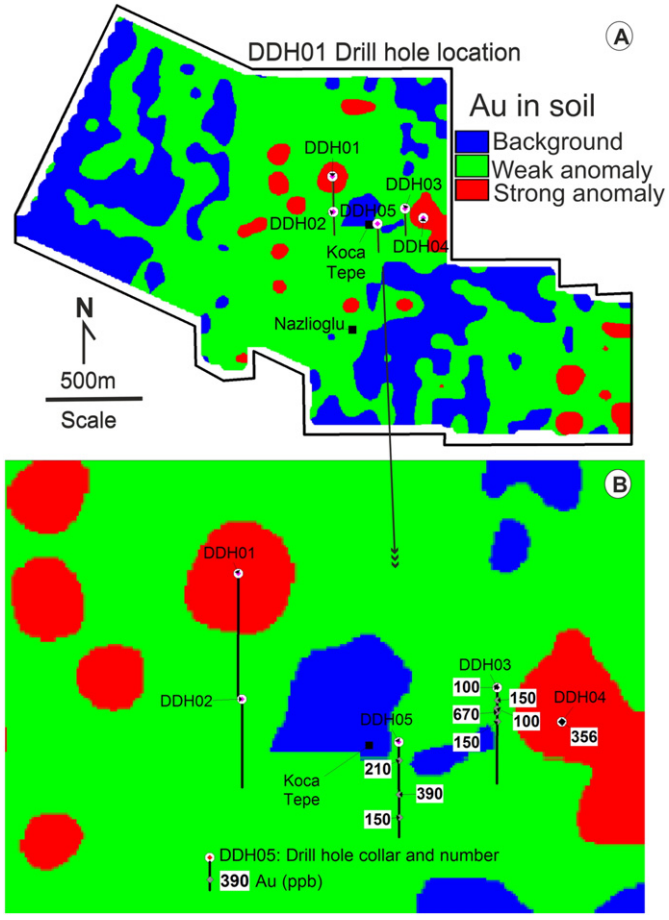

Fig. 14. Phase I diamond drill holes (DDH) location in conventional soil anomaly map (A) and a closer view of Au contents from the DDH in relation to soil gold anomalies.

layers at depths ranging from 7 to 119 m (Figs. 13C and 15B). More interestingly, DDH10 drill hole was designed to test a strong MMI soil anomaly (AuRR >76) and returned Au values of 230 ppb and 400 ppb from depths of 78 m and 400 ppb (Fig. 13C). MMI AgRR anomalies partially coincide with those of Au (Fig. 13D). The best drill core Ag intersection yielded that 1 m@363 ppm was from DDH11 at 105 m depth.

6. Discussion

BLEG stream sediment geochemical sampling is a time- and cost-efficient method in assessing a large moderately rugged terrain (250 km2 in this case). Whereas the collection of 40 BLEG samples took six days, collection of 1000–80 mesh stream samples (4 samples/1 km^2) may take 70 working days or 3 months from the same area. Bulk cyanide leaching of large samples (2 kg/−16 mesh or 1 kg/−80 mesh fractions) overcomes the probability that fine gold grains are not distributed heterogeneously within a sample. Accordingly, −80 mesh BLEG samples yielded strong Au and Ag anomalies with averages of 6.2 and 29.8 ppb, respectively, which are 3.5 and 2.1 times greater than those of −16 mesh BLEG samples. However, collection of 40–80 mesh BLEG samples may take considerably longer time.

BLEG (−16 mesh and −80 mesh) and −80 mesh stream sediment geochemical sampling carried out in the Cemalcavus area proved to be highly efficient in detecting even weak Au/Ag mineralization. It has been shown by many authors that geochemical data show neither normal nor log-normal distributions (Rawlins et al., 2012; Reimann and Filzmoser, 2000). Carranza (2010) stated that although percentiles of values in any data set were robust despite their empirical frequency distributions, visual inspection of spatial distributions of percentile-based classes of dilution-corrected uni-element residuals is also arguably subjective. However, robust C–A fractal analysis (Carranza, 2010) of BLEG sample results identified several weak BLEG Au and Ag anomalies (Fig. 7). Follow-up of the BLEG anomalies gave rise to a dozen of moderate to strong −80 mesh stream sediment Au and As anomalies, which

Table 5
Selected trace element geochemistry for drill core samples from the Cemalcavus area.

Sample	*Au	Ag	As	Sb	Cu	Pb	Zn	DDH	Dip (°)	From (m)	To (m)	True depth (m)
3460	100	1.2	161	4.3	54	59	97	DDH03	65	8	9	7.2
3489	150	0.2	42	0.7	38	18	101	DDH03	65	38	39	34.4
3524	100	0.1	16	0.6	33	13	70	DDH03	65	73	74	66.1
3526	670	0.7	160	4.0	37	18	200	DDH03	65	75	76	67.9
3650	150	0.1	277	0.7	34	10	46	DDH03	65	99	100	89.7
3772	130	0.53	143	3.2	21	16	78	DDH04	90	20	21	20
3774	130	1.14	144	4.6	65	21	109	DDH04	90	22	23	22
3796	200	0.57	235	15.0	35	16	93	DDH04	90	44	45	44
3830	170	0.27	48.8	1.5	20	17	88	DDH04	90	78	79	78
4650	700	0.23	24.4	0.6	44	11	58	DDH04	90	197	198	197
4665	810	1.31	6840	1.7	33	9	64	DDH04	90	212	213	212
4810	210	1.3	95	1.8	7	9	64	DDH05	65	66	67	59.7
4934	390	1.2	3	0.8	51	21	112	DDH05	65	190	191	172.0
4984	150	0.1	4	0.4	8	7	29	DDH05	65	238	239	215.6
7587	110	0.3	642	19.2	48	20	139	DDH08	60	36	37	31.0
7688	280	0.7	157	5.1	25	15	77	DDH08	60	136	137	117.0
7716	150	2.5	389	9.9	181	22	86	DDH09	60	30	31	25.8
7717	280	2.6	413	14.4	54	13	55	DDH09	60	31	32	26.7
7789	240	0.8	717	32.4	26	17	53	DDH09	60	105	106	91.2
7791	190	0.5	429	19.3	35	12	53	DDH09	60	107	108	92.0
7825	120	0.3	221	3.8	57	14	80	DDH09	60	139	140	119.5
7954	230	8.1	284	4.5	623	99	125	DDH10	55	96	97	78.6
7993	400	0.6	46	1.3	20	16	60	DDH10	55	136	137	111.4
9056	120	3.0	250	16.6	512	37	111	DDH11	50	10	11	7.6
9132	100	0.2	298	4.0	39	17	107	DDH11	50	85	86	64.6
9138	140	0.5	339	4.3	8	15	70	DDH11	50	91	92	69.9
9185	90	363.0	126	2.5	1500	40	81	DDH11	50	138	139	104.8
9186	110	35.6	171	4.9	231	28	82	DDH11	50	139	140	105.6
9200	10	11.2	27	1.0	70	21	107	DDH11	50	153	154	116.3
9651	130	0.3	268	5.4	56	15	90	DDH16	55	12	14	9.1
9658	110	0.4	309	10.5	47	20	111	DDH16	55	26	28	19.8

* All in ppm except for Au in ppb.

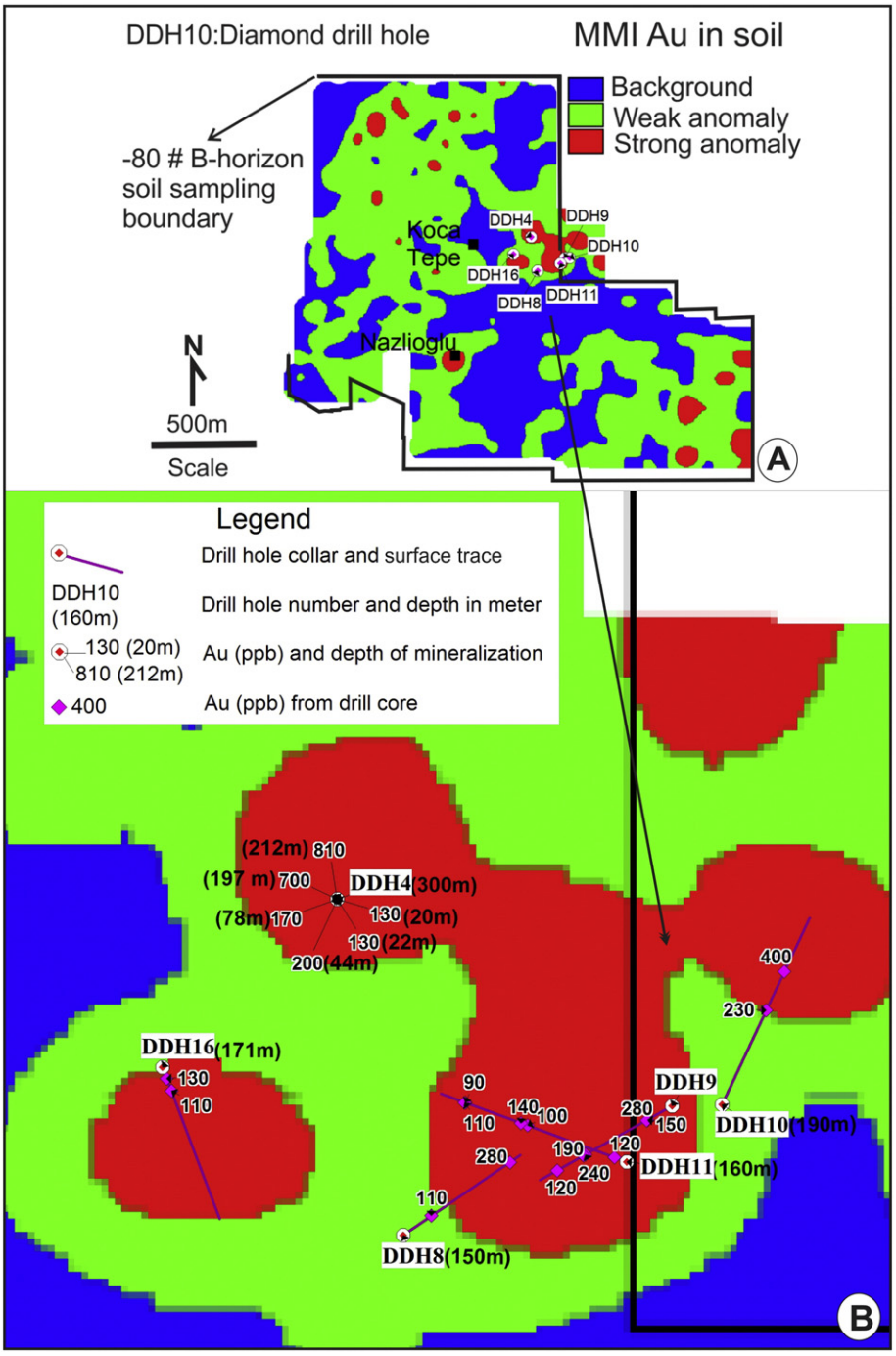

Fig. 15. Phase II diamond drill holes (DDH) location in MMI soil anomaly map (A) and a closer view of Au contents from the DDH in relation to soil gold anomalies.

were also defined by robust C–A fractal analysis (Figs. 9 and 10). Threshold values for Au, As, Cu and Zn defined by *median + 2MAD* method are much higher (almost two-fold) than those defined by C–A fractal analysis (Figs. 9A, C, E, G and 10 A, C, E, G; Table 2).

A cluster of −80 mesh stream sediment anomalies is a significant guide for Au mineralization in the Cemalcavus prospect. Single −80 mesh stream sediment anomalies have not yet led to discovery of any Au–Ag mineralization in the area. Minus 80 mesh stream sediment data from Cemalcavus confirm the strong spatial association of Au with As (Figs. 9B, D and 10B, D). Also important was spatially strong associations of Au with As in conventional soil (Fig. 11B, D) and Cu in MMI soil (Fig. 12B, F). Silver is a useful indicator element for Au at both regional (BLEG; Fig. 7D) and local (MMI soil; Fig. 13B) scales although ICP data obtained from commercial laboratories generally have too high a detection limit for more subtle anomalies such as at Cemalcavus. Conventional soil B-zone geochemical sampling method may be ineffective for detecting blind mineral deposits when these occur deep within sequences of stable-platform carbonates and shales (Mann et al., 1998). In deep lateritic weathering profiles where element mobility both vertically and laterally can be substantial, elevated anomalous responses at or near the surface often does not necessarily reflect primary or higher grade mineralization directly below. MMI geochemistry speculates that physical (e.g., capillary rise) and electrochemical processes liberate mobile metal ions from a buried mineral deposit, which migrate to the surface where they are weakly attached to soil particles (Amedjoe and Adjovu, 2013; Goldberg, 1998; Mann et al.,

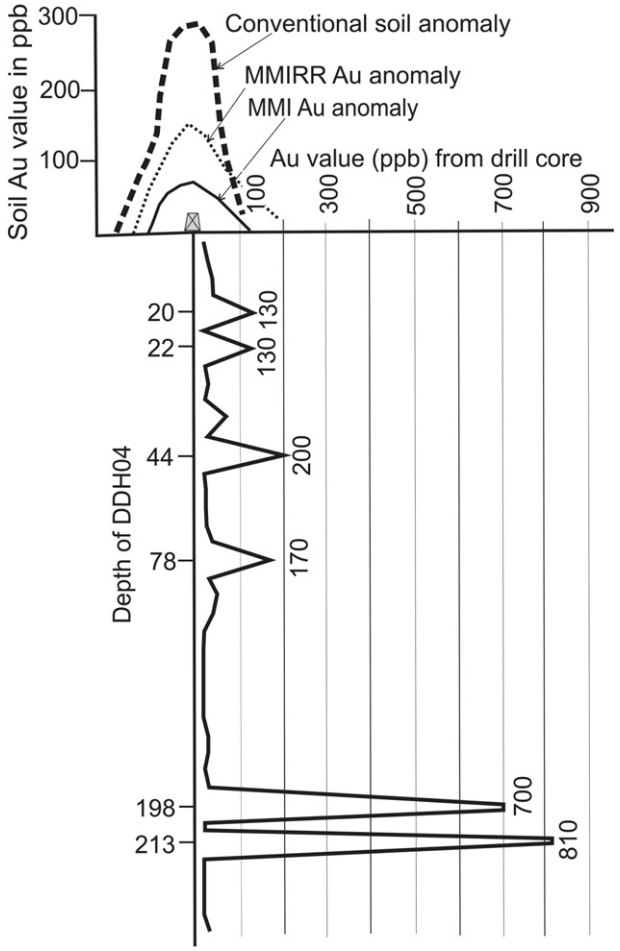

Fig. 16. Variation of low-grade DDH04 Au values and their relation to conventional and MMI soil Au anomalies.

2005). In the study area, strong MMI soil Au anomalies predominate in the northwestern and southeastern ends, and central part whereas major strong As anomalies dominate in the southeast end (Fig. 11B and D). In the Cemalcavus area, discovery of buried Au mineralization at depths, ranging from 8 to 212 m, by strong MMI soil anomalies is not a coincidence. In particular, the DDH10 intersected the Au mineralization at depths of 97 m and 137 m where only a 30 times MMI response ratio contour soil anomaly led to discovery of an indisputable buried Au mineralization. The drill core sections of DDH04 from 1 m to 12 m and from 13 m to 19 m returned average Au values of 5 ppb and 10 ppb with peak Au values of 5 and 40 ppb, respectively. Therefore, mineralization at these depths cannot be detected by conventional soil sampling method. Furthermore, DDH04 includes 200, 700 and 810 ppb Au values at depths of 44, 197 and 215 m, respectively, and these are also expected to have contributed to the Au budget of the strong MMI anomaly.

7. Conclusions

The discovery of the Cemalcavus prospect during the follow-up of a BLEG anomaly is an exploration success using −80 mesh stream sediment as well as conventional and MMI soil geochemistry. Concentration–area (C–A) fractal modeling of raw geochemical data generated six weak BLEG Au anomalies. Follow-up of the BLEG anomalies by −80 mesh stream sediment geochemical sampling led to identification of Au mineralization centered at Koca Tepe location. Conventional −80 mesh soil sampling failed to detect any buried Au–Ag mineralization, the closest of which was intersected at 7 m depth, e.g., DDH03 and DDH11. Gold anomalies detected by the conventional −80 mesh soil technique were probably formed by early stage as mobile metal ions, which were ultimately bind to soil, e.g., as iron oxy-hydroxides in soil profiles. The MMI soil technique has further demonstrated its superiority over the conventional −80 mesh soil sampling technique, as proven by the mineralized diamond drill hole Au–Ag intercepts.

A combination of BLEG and −80 mesh stream sediment techniques played an indisputable role in the discovery of the Cemalcavus Au–Ag–As anomaly during green-field exploration in the area where no Au/Ag mineralization was previously recorded in published or unpublished literature or known by locals. However, an economically viable Au or base metal deposit is yet to be discovered in the area.

Acknowledgments

I would like to express my appreciation to Ege Madencilik (Project number 10), Turkey for financial support to the project during my presence as Operating Manager. Nick Greenfield and reviewers D. Jason and an anonymous reviewer are thanked for their invaluable comments that helped improve the quality of this paper.

References

Afzal, P., Khakzad, A., Moarefvand, P., Omran, N.R., Esfandiari, B., Alghalandis, F.Y., 2010. Geochemical anomaly separation by multifractal modeling in Kahang (Gor Gor) porphyry system, Central Iran. J. Geochem. Explor. 104, 34–46.

Akiska, S., Ünlü, T., Sayılı, S., 2008. İzmir-Ödemiş yöresindeki arsenopiritli altın oluşumlarının maden jeolojisi. MTA Dergisi 136, 1–8.

Amedjoe, C.G., Adjovu, Isaac T., 2013. Application of the mobile metal ion geochemical technique in the location of buried gold mineralization in Essase Concession, Eastern Region, Ghana. J. Geol. Min. Res. http://dx.doi.org/10.5897/JGMR2013.0175.

Arias, M., Gumiel, P., Martín-Izard, A., 2012. Multifractal analysis of geochemical anomalies: A tool for assessing prospectivity at the SE border of the Ossa Morena Zone, Variscan Massif (Spain). J. Geochem. Explo. 122, 101–112.

Asadi, H.A., Kianpouryan, S., Lu, Y.-J., McCuaig, T.C., 2013. Exploratory data analysis and C–A fractal model applied in mapping multi-element soil anomalies for drilling: a case study from the Sari Gunay epithermal gold deposit, NW Iran. J. Geochem. Explor. 145, 233–241.

Bajc, A.F., 1997. A comparative analysis of enzyme leach and mobile metal ion selective extractions; case studies from glaciated terrain, northern Ontario. J. Geochem. Explor. 61, 113–148.

Beeson, R., 1995. A drainage sediment geochemical orientation study at Boddington, Western Australia. J. Geochem. Explor. 54, 63–71.

Beus, A.A., Grigorian, S.V., 1977. Geochemical Exploration Methods for Mineral Deposits. Applied Publishing Ltd., Illinois, USA.

Cağatay, A., Eyyüboğlu, T., 1979. On the mineralogical and brief geological investigations, and genetic data of some antimony arsenopyrite, cinnabar and scheelite deposits and occurrences in western Anatolia. Bull. Chamber Geol. Eng. 9, 51–62 (in Turkish).

Cameron, E.M., Leybourne, M.I., Kelley, D.L., 2002. Exploring for deeply covered mineral deposits: formation of geochemical anomalies in northern Chile by earthquake-induced surface flooding of mineralized groundwaters. Geology 30, 1007.

Cameron, E.M., Hamilton, S.M., Leybourne, M.I., Hall, G.E.M., McClenaghan, B., 2004. Finding deeply buried deposits using geochemistry. Geochem. Explor. Environ. Anal. 4, 7–32.

Candan, O., Dora, O.Ö., Oberhänsli, R., Çetinkaplan, M., Partzsch, J.H., Warkus, F., Durr, S., 2001. Pan-African high-pressure metamorphism in the Precambrian basement of the Menderes Massif, western Anatolia, Turkey. Int. J. Earth Sci. 89 (4), 793–811.

Candan, O., Oberhansli, R., Dora, O.Ö., Çetinkaplan, M., Koralay, E., Rimmele, G., Chen, F., Akal, C., 2011. Polymetamorphic evolution of the Pan-African Basement and Palaeozoic–Early Tertiary cover series of the Menderes Massif. Bull. Mineral Res. Explor. Inst. Turk. 142, 121–163.

Carlile, J.C., Davey, G.R., Kadir, I., Langmead, R.P., Rafferty, W.J., 1998. Discovery and exploration of the Gosowong epithermal gold deposit, Halmahera, Indonesia. J. Geochem. Explor. 60, 207–227.

Carranza, E.J.M., 2009. Geochemical anomaly and mineral prospectivity mapping in GIS. Handbook of Exploration and Environmental Geochemistry 11. Elsevier (351 pp.).

Carranza, E.J.M., 2010. Catchment basin modelling of stream sediment anomalies revisited: incorporation of EDA and fractal analysis. Geochem. Explor. Environ. Anal. 10, 365–381.

Cheng, Q., Agterberg, F.P., Ballantyne, S.B., 1994. The separation of geochemical anomalies from background by fractal methods. J. Geochem. Explor. 51, 109–130.

Cohen, D.R., Dunlop, A.C., Rose, T., 2004. Contrasting dispersion patterns for gold in stream sediments at Timbarra, NSW. Aust. J. Geochem. Explor. 85, 1–16.

Cohen, D.R., Kelley, D.L., Anand, R., Coker, W.B., 2010. Major advances in exploration geochemistry, 1998–2007. Geochem. Explor. Environ. Anal. 10, 3–16.

Collins, A.S., Robertson, A.H.F., 2003. Kinematic evidence for Late Mesozoic–Miocene emplacement of the Lycian Allochthon over the Western Anatolide Belt, SW Turkey. Geol. Mag. 38, 295–310.

El-Makky, A.M., Sediek, K.N., 2012. Stream sediments geochemical exploration in the northwestern part of Wadi Allaqi Area, South Eastern Desert, Egypt. Nat. Resour. Res. 21, 95–115.
Ercan, T., Dincel, A., Metin, S., Turkecan, A., Gunay, A., 1978. Usak yoresinde Neojen havzalarinin jeolojisi. T.J.K. Bulteni 21/2, 97–106.
Eurogold Company., 1992. Report on gold anomaly summary in Menderes Massif, Turkey, 109 pp. (Unpublished report).
Fletcher, W.K., 1997. Stream sediment geochemistry in today's exploration world. In: Gubins, A.G. (Ed.), Proceedings of Exploration'97-4th Decennial International Conference on Mineral Exploration, pp. 249–260.
Fletcher, K., Horskey, S., 1988. Determination of gold by cyanidation and graphite furnace atomic absorption spectroscopy. J. Geochem. Explor. 30, 29–34.
Goldberg, I.S., 1998. Vertical migration of elements from mineral deposits. J. Geochem. Explor. 61, 191–202.
Goncalves, M.A., Mateus, A., Oliveira, V., 2001. Geochemical anomaly separation by multifractal modelling. J. Geochem. Explor. 72, 91–114.
Govett, G.J.S., 1976. Detection of deeply buried and blind sulfide deposits by measurement of H+ and conductivity of closely spaced surface soil samples. J. Geochem. Explor. 6, 359–382.
Gray, D.J., Wildman, J.E., Longman, G.D., 1999. Selective and partial extraction analyses of transported overburden for gold exploration in the Yilgarn Craton, Western Australia. J. Geochem. Explor. 67, 51–66.
Hale, M., Plant, J.A., 1994. Drainage geochemistry. In: Govett, G.J.S. (Ed.), Handbook of Exploration Geochemistry vol. 6. Elsevier, Amsterdam.
Hao, L., Zhao, X., Zhao, Y., Lu, J., Sun, L., 2014. Determination of the geochemical background and anomalies in areas with variable lithologies. J. Geochem. Explor. 139, 177–182.
Hetzel, R., Passchier, C.W., Ring, U., Dora, O., 1995. Bivergent extension in orogenic belts: the Menderes Massif (southwestern Turkey). Geology 23, 455–458.
Hetzel, R., Romer, R.L., Candan, O., Passchier, C.W., 1998. Geology of the Bozdag area, central Menderes Massif, SW Turkey: Pan-African basement and Alpine deformation. Int. J. Earth Sci. 87, 394–406.
Kelley, D.L., Hall, G.E.M., Closs, L.G., Hamilton, I.C., McEwen, R.M., 2003. The use of partial extraction geochemistry for copper exploration in northern Chile. Geochem. Explor. Environ. Anal. 3, 85–104.
Klusman, R.W., 2009. Transport of ultratrace reduced gases and particulate, near-surface oxidation, metal deposition and adsorption. Geochem. Explor. Environ. Anal. 9, 203–213.
Koralay, O.E., Satir, M., Dora, O., 2001. Geochemical and geochronological evidence for Early Triassic calc-alkaline magmatism in the Menderes Massif, western Turkey. Int. J. Earth Sci. 89, 822–835.
Leduc, C., Itard, Y., 2003. Low sampling density exploration geochemistry for gold in arid and tropical climates: comparison between conventional geochemistry and BLEG. Geochem. Explor. Environ. Anal. 3, 121–131.
Levinson, A.A., 1974. Introduction to Exploration Geochemistry. Applied Publishing Ltd., Wilmette, IL.
Li, C.J., Ma, T.H., Shi, J.F., 2003. Application of a fractal method relating concentrations and distances for separation of geochemical anomalies from background. J. Geochem. Explor. 77, 167–175.
Lusty, P.A.J., Scheib, C., Gunn, A.G., Walker, S.D., 2012. Reconnaissance-scale prospectivity analysis for gold mineralisation in the Southern Uplands-Down-Longford Terrane, Northern Ireland. Nat. Resour. Res. 21, 359–382.
Luz, F., Mateus, A., Matos, J.X., Gonçalves, M.A., 2014. Cu- and Zn-soil anomalies in the NE border of the South Portuguese Zone (Iberian Variscides, Portugal) identified by multifractal and geostatistical analyses. Nat. Resour. Res. 23, 195–215.
Mann, A.W., Birrell, R.D., Mann, A.T., Humphreys, D.B., Perdrix, J.L., 1998. Application of the mobile metal ion technique to routine geochemical exploration. J. Geochem. Explor. 61, 87–102.
Mann, A.W., Birrell, R.D., Fedikow, M.A.F., Souza, H.A.F., 2005. Vertical ionic migration: soil anomalies, and sampling depth for mineral exploration. Geochem. Explor. Environ. Anal. 5, 201–210.
Mazzucchelli, R., 1990. Advanced exploration geochemistry. Workshop Course 704/90. Australian Mineral Foundation, Australia. Publication No. 550.84.
Meier, A.L., 1980. Flameless atomic-absorption determination of gold in geological materials. J. Geochem. Explor. 13, 77–85.
MTA (Maden Tetkik ve Arama Enstitüsü), 1970. Arsenic, Mercury, Antimony and Gold Deposits of Turkey. MTA Publications 129, Ankara.
MTA (Maden Tetkik ve Arama Enstitusu), 1979. Türkiye antimon dökümü. MTA yayınları 129, Ankara.
Nyade, P.K., Wilton, D.H.C., Longerich, H.P., Thompson, G.M., McNeil, P., 2011. Use of surficial geochemical methods to locate areas of buried uranium mineralization in the Jacque's Lake area of the Central Mineral Belt, Labrador, Canada. Can. J. Earth Sci. 50, 1134–1146.
Putikov, O., Wen, B., 2000. Geoelectrochemistry and stream dispersion. Handb. Explor. Geochem. 7, 17–79.
Radford, N., 1996. BLEG sampling in gold exploration: an Australian view. Explore 92, 8–10.
Rawlins, B.G., McGrath, S.P., Scheib, A.J., Breward, N., Cave, M., Lister, T.R., Ingham, M., Gowing, C., Carter, S., 2012. The Advanced Soil Geochemical Atlas of England and Wales. British Geological Survey, Nottingham, UK (227 pp.).
Regnier, Jean-Luc.L., Mezger, J.E., Passchier, C.W., 2007. Metamorphism of Precambrian–Palaeozoic schists of the Menderes core series and contact relationships within Proterozoic orthogneisses of the western Cine Massif, Anatolide belt, western Turkey. Geol. Mag. 144/1, 67–104.
Reimann, C., Filzmoser, P., 2000. Normal and lognormal data distribution in geochemistry: death of a myth. Consequences for the statistical treatment of geochemical and environmental data. Environ. Geol. 39, 1001–1014.
Reimann, C., Garrett, R.G., 2005. Geochemical background—concept and reality. Sci. Total Environ. 350, 12–27.
Reith, F., Mcphail, D.C., 2007. Mobility and microbially mediated mobilization of gold and arsenic in soils from two gold mines in semi-arid and tropical Australia. Geochim. Cosmochim. Acta 71, 1183–1196.
Reyes, A.G., 1991. Mineralogy, distribution and origin of acid alteration in Philippine geothermal system. Geol. Surv. Japan 77, 59–65.
Rimmele, G., Oberhansli, R., Goffe, B., Jolivet, L., Candan, O., Cetinkaplan, M., 2003. First evidence of high-pressure metamorphism in the "Cover Series" of the southern Menderes Massif. Tectonic and metamorphics implications for the evolution of SW Turkey. Lithos 71, 19–46.
Rimmele, G., Parra, T., Goffe, B., Oberhansli, R., Jolivet, L., Candan, O., 2005. Exhumation paths of high-pressure–low-temperature metamorphic rocks from the Lycian Nappes and the Menderes Massif (SW Turkey): a multi-equilibrium approach. J. Petrol. 46, 641–669.
Rose, A.W., Hawks, H.E., Webb, J.H., 1979. Geochemistry in Mineral Exploration. Academic Press, NY, USA.
Sengor, A.M.C., Satir, M., Akkok, R., 1984. Timing of tectonic events in the Menderes Massif, western Turkey: implications for tectonic evolution and evidence for Pan-African basement in Turkey. Tectonics 3, 693–707.
Smee, B.W., 1983. Laboratory and field evidence in support of the electrogeochemically enhanced migration of ions through glaciolacustrine sediment. J. Geochem. Explor. 19, 277–304.
Sonmez, F.N., 2013. Menderes Masifi (Batı Anadolu) altin içeren arsenopiritli kuvars damarlarinin yapısal ozellikleri, izotop jeokimyası ve sivi kapanimlarinin incelenmesi. Dokuz Eylul Universitesi BAP Project.
Taylor, S.R., 1966. The application of trace element data to problems in petrology. Phys. Chem. Earth 6, 133–213.
Thompson, M., Howarth, R.J., 1978. A new approach to the estimation of analytical precision. J. Geochem. Explor. 9, 23–30.
Tukey, J.W., 1977. Exploratory Data Analysis. Addison-Wesley, Reading.
White, N.C., Hedenquist, J.W., 1995. Epithermal gold deposits: styles, characteristics and exploration. Soc. Econ. Geol. 23, 9–13.
Xueqiu, W., Xuejing, X., Zhizhong, C., Dawen, L., 1999. Delineation of regional geochemical anomalies penetrating through thick cover in concealed terrains— a case history from the Olympic Dam deposit, Australia. J. Geochem. Explor. 66, 85–97.
Yigit, O., 2009. Mineral deposits of Turkey in relation to Tethyan metallogeny: implications for future mineral exploration. Econ. Geol. 104, 19–51.
Yilmaz, H., 2003. Geochemical exploration for gold in western Turkey: success and failure. J. Geochem. Explor. 80, 117–135.
Yilmaz, H., 2007. Stream sediment geochemical exploration for gold in the Kazdağ Dome in the Biga Peninsula, Western Turkey. Turk. J. Earth Sci. 16, 33–55.
Yilmaz, H., Sonmez, F.N., Sener, A.K., Tezel-Tufan, S., 2013. Low-sulfidation type Au–Ag mineralization at Sindirgi, Balikesir, Turkey. Turk. J. Earth Sci. 22, 485–522.
Yousefi, M., Carranza, E.J.M., Abolghasem Kamkar-Rouhani, A., 2013. Weighted drainage catchment basin mapping of geochemical anomalies using stream sediment data for mineral potential modeling. J. Geochem. Explor. 128, 88–96.